Review

Tengfei Shi, Shahid Hussain*, Chuanxin Ge, Guiwu Liu*, Mingsong Wang and Guanjun Qiao*

ZIF-X (8, 67) based nanostructures for gas-sensing applications

https://doi.org/10.1515/revce-2021-0100
Received December 15, 2021; accepted April 23, 2022;
published online June 15, 2022

Abstract: ZIF-8 and ZIF-67 are the most investigated zeolitic imidazolate frameworks (ZIFs) materials that have aroused enormous scientific interests in numerous areas of application including electrochemistry, gas storage, separation, and sensors by reason of their fascinating structural properties. Recently, there is a rapidly growing demand for chemical gas sensors for the detection of various analytes in widespread applications including environmental pollution monitoring, clinical analysis, wastewater analysis, industrial applications, food quality, consumer products, and automobiles. In general, the key to the development of superior gas sensors is exploring innovative sensing materials. ZIF-X (8, 67) based nanostructures have demonstrated great potential as ideal sensing materials for high-performance sensing applications. In this review, the general properties and applications of ZIF-X (8, 67) including gas storage and gas adsorption are first summarized, and then the recent progress of ZIF-X (8, 67) based nanostructures for gas-sensing applications and the structure-property correlations are summarized and analyzed.

Keywords: gas sensors; metal-organic frameworks; nanostructures; ZIF-X (8, 67).

***Corresponding authors: Shahid Hussain and Guiwu Liu**, School of Materials Science and Engineering, Jiangsu University, Zhenjiang, 212013, China, E-mail: shahid@ujs.edu.cn (S. Hussain), gwliu76@ujs.edu.cn (G. Liu); and **Guanjun Qiao**, School of Materials Science and Engineering, Jiangsu University, Zhenjiang, 212013, China; and State Key Laboratory for Mechanical Behavior of Materials, Xi'an Jiaotong University, Xi'an 710049, China, E-mail: gjqiao@ujs.edu.cn (G. Qiao)
Tengfei Shi, Chuanxin Ge and Mingsong Wang, School of Materials Science and Engineering, Jiangsu University, Zhenjiang, 212013, China

1 Introduction

Over the previous decades, the development and practical application of porous materials have been one of the critical tasks of modern technologies (e.g., separation technologies). The family of porous materials has been dramatically expanded by numerous new types of porous materials, such as zeolite-type, carbon nanotubes, activated carbon, and porous metal–organic materials. Metal organic frameworks (MOFs) are one of the hot materials in the field of porous nanomaterials, which are constructed by linking single-metal cations or metal clusters with organic linkers (Furukawa et al. 2013; Li et al. 2012; Wang et al. 2018c; Yuan et al. 2018). To date, numerous facile synthesis routes have been developed to prepare MOFs, such as solvothermal/hydrothermal (Soltanolkottabi et al. 2020; Zhang et al. 2020b), microwave-assisted (Lucero et al. 2020; The Ky et al. 2019; Xu et al. 2020b), mechanochemical (Brekalo et al. 2020; Chen et al. 2020; Li et al. 2014b), electrochemical (Martinez Joaristi et al. 2012; Stock and Biswas 2012), sonochemical (Othong et al. 2019; Soleimani et al. 2020) and microfluidic methods (Faustini et al. 2013; Hu et al. 2020; Wu et al. 2019a). Owing to the features of their crystalline structure, MOFs are also considered ideal templates for the derivation of various porous materials such as carbonaceous materials, metal compounds, and their composites (Kaneti et al. 2017; Salunkhe et al. 2017; Shen et al. 2016; Wang et al. 2018a; Yan et al. 2018; Zhang et al. 2019f). MOFs based nanomaterials have been widely applied in numerous fields, including gas storage, gas separation, biomedical imaging, energy storage, catalysis, drug delivery, chemical sensors, and others (Adatoz et al. 2015; Dong et al. 2022; Kong et al. 2012; Koo et al. 2019; Kreno et al. 2011; Li et al. 2012, 2018b, 2019, 2020a, 2021; Mason et al. 2014; Pham et al. 2020; Taheri et al. 2021; Wu et al. 2020; Yang and Yang 2020; Zhang et al. 2021).

Zeolitic imidazole frameworks (ZIFs) are an exceptional subfamily of MOFs composed of inorganic metal cations (M^{2+}) and imidazolate-type ligands (Park et al. 2006). The representative ZIFs framework structures in previous reports are displayed in Figure 1. Recently, ZIFs have been widely studied for several applications due to their promising features including ultra-large surface area,

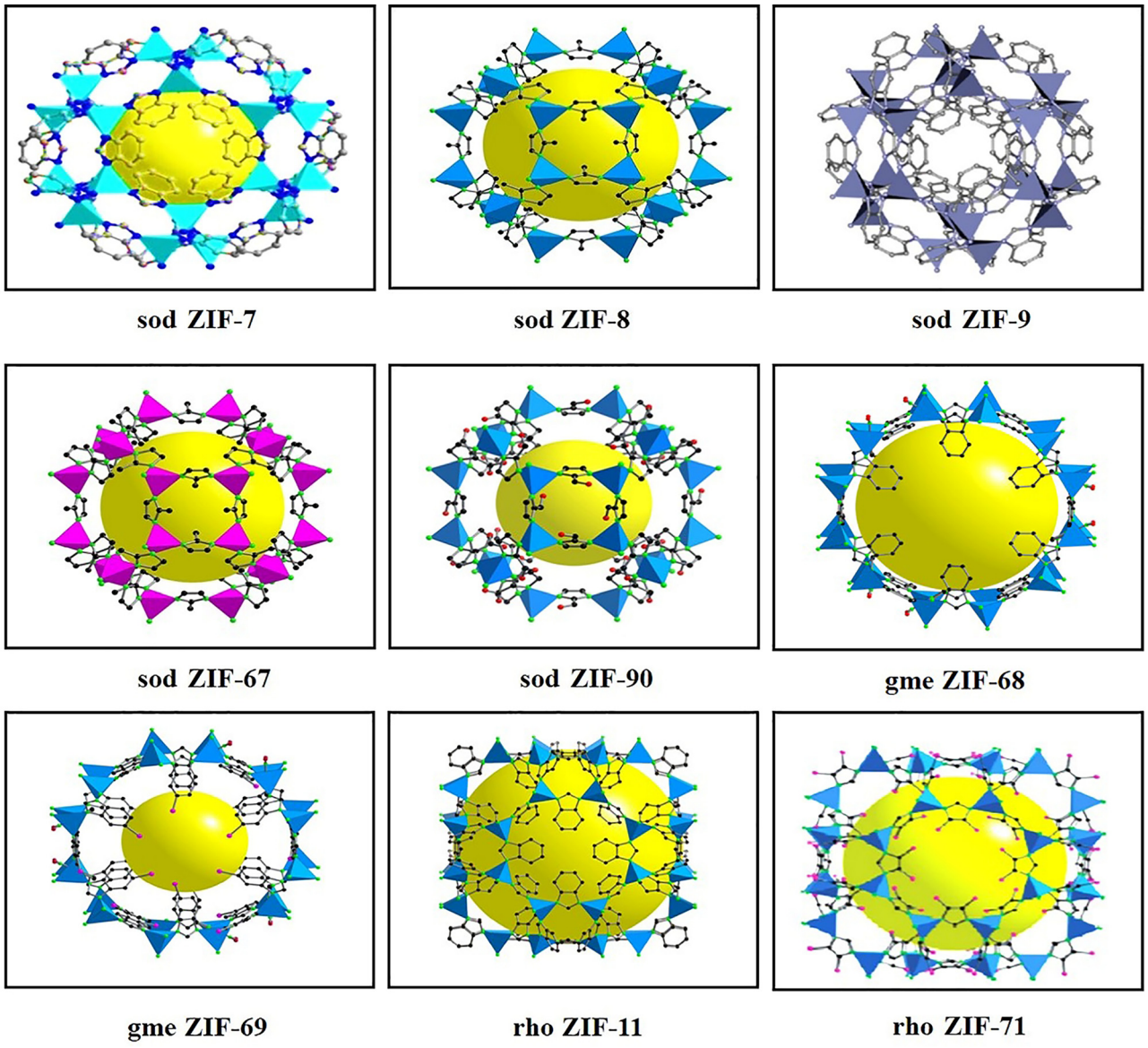

Figure 1: The framework structures of ZIFs (Anh Phan et al. 2009; Ying et al. 2015; Zakzeski et al. 2011). Copyright permission obtained to reproduce from RSC Publishing, Elsevier and American Chemical Society.

exceptionally high hydrothermal robustness, and excellent chemical resistance (Guo et al. 2010; Han et al. 2018; Pan et al. 2012; Song et al. 2020; Sun et al. 2012; Xu et al. 2017). To date, more than 150 novel ZIFs structures have been synthesized, some of which exhibit structures topology similar to zeolites, and others also can be found in materials different from traditional zeolites (Anh Phan et al. 2009). Figure 2 shows the number of research publications about "ZIF" and "gas sensing" from the Web of Science. As can be seen from Figure 2, ZIF-8 and ZIF-67 are the most studied materials among numerous ZIFs. Both ZIF-8 and ZIF-67 with a sodalite topology are isostructural with zeolites, and they have similar lattice parameters and the same 2-methylimidazole organic ligands, but they use different metal centers (Zn^{2+} or Co^{2+}) to build their structures.

As the most popular materials among numerous ZIFs materials, ZIF-8 and ZIF-67 possess extremely stable structures, giant surface areas, controllable pore apertures, tunable morphologies, and easily synthesis. Inspired by these charming characteristics, ZIF-X (8, 67) based nanostructures have been further employed as ideal sensing elements for gas-sensing applications. Further, compared with other common sensing materials (e.g., semiconductor metal oxide, conducting polymer, and graphene), ZIF-X (8, 67) based nanostructures exhibit high sensitivity,

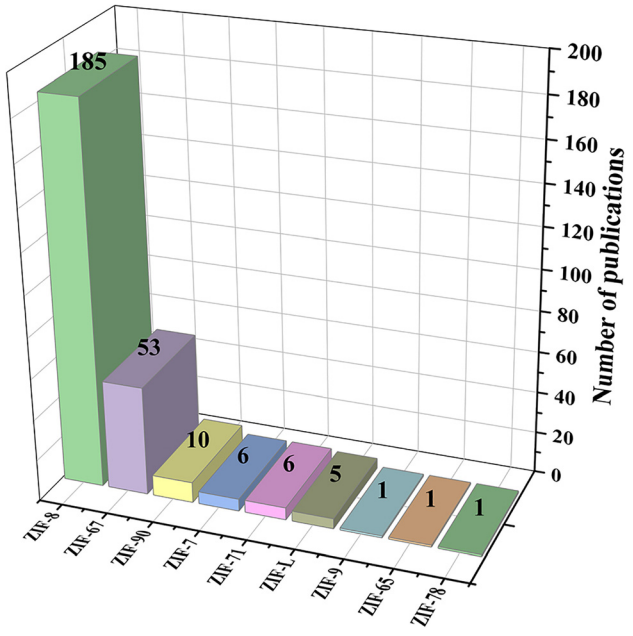

Figure 2: Trends in ZIF publication.

excellent gas selectivity, and good stability, while pure ZIFs tend to exhibit low sensitivity due to their poor electrical conductivity. However, the derivatives from ZIF-X (8, 67) and semiconductor metal oxide gas sensors tend to have a high operating temperature, while graphene and conducting polymer gas sensors can operate at room temperature, but their sensitivity and selectivity are poor.

So far, a number of excellent reviews on synthesis, properties, and sensing applications (e.g., optical chemical sensing, electrochemical sensing (Liu et al. 2020), metal ion sensing and biosensing (Kukkar et al. 2021) of ZIFs have been published). However, there is no dedicated review on ZIF-X (8, 67) based nanostructures (e.g., pure ZIFs, ZIFs composites, and derivatives) for gas sensing applications. In this review, we systematically summarize the ongoing progresses of ZIF-X (8, 67) based nanostructures for gas-sensing applications. First, we discuss the structural characteristics of the ZIF-X (8, 67) materials, such as surface area, tunable structures, stability. Then, the general properties (chemical and physical properties) and applications (gas storage and gas separations) of ZIF-X (8, 67) have been examined. In the third part, we detail the preparation process, sensing performances, and the sensing mechanism of the ZIF-X (8, 67) based nanostructures, especially focusing on the structure-property relationship. All gas sensors utilizing ZIF-X (8, 67) based nanostructures as the gas-sensing materials can be divided into two groups: volatile organic compounds (VOCs) sensor and inorganic gas sensor. Finally, the prevailing challenges and future research regarding ZIF-X (8, 67) based nanostructures for gas-sensing applications are also summarized.

2 The structure of ZIF-X (8, 67)

In recent years, numerous different strategies have been studied to design and tune the particle sizes and morphologies of ZIFs, and some classic morphologies of ZIFs are summarized in Table 1. The manipulation of particle sizes and morphologies of ZIFs is significant for optimizing the properties of the ZIFs and their derivatives. Therefore, Pan et al. (2011) have developed a facile method to change the morphology of ZIF-8 nanocrystals from the typical rhombic dodecahedron to truncated cubic and truncated rhombic dodecahedron, and various morphologies of ZIF-8 nanocrystals were shown in Figure 3A–D. This approach is based on precisely controlling the concentration of surfactant cetyltrimethylammonium bromide to achieve morphological control. Hollow nanostructures have been extensively studied for their quite important practical applications in recent years. Li et al. (2015) reported that the unique hierarchical porous ZnO hollow cubes structure could be constructed by directly decomposing ZIF-8 with cube-like morphology. The as-prepared ZnO nanostructure possesses excellent structural properties (e.g., high surface area) owing to maintaining the original structure of the ZIF-8 precursors. Besides, Xu et al. (2016) have demonstrated that the hollow ZIF-8 spheres with

Table 1: The morphologies of representative ZIFs in previous reports.

ZIF-n	Composition	Net	Morphology	References
8	$Zn(MeIM)_2$	Sod	Rhombic dodecahedra	Torad et al. (2013)
8	$Zn(MeIM)_2$	Sod	Truncated rhombic dodecahedral	Pan et al. (2011)
8	$Zn(MeIM)_2$	Sod	Cube-like	Li et al. (2015)
8	$Zn(MeIM)_2$	Sod	Hollow spheres	Lee et al. (2012) and Xu et al. (2016)
8	$Zn(MeIM)_2$	Sod	Cage-like	Zhang et al. (2019d)
67	$Co(MeIM)_2$	Sod	Rhombic dodecahedra	Guo et al. (2016)
67	$Co(MeIM)_2$	Sod	Truncated rhombic dodecahedral	Guo et al. (2016)
67	$Co(MeIM)_2$	Sod	Hollow prisms	Yu et al. (2016)
67	$Co(MeIM)_2$	Sod	Nanotube	Yu et al. (2015)
67	$Co(MeIM)_2$	Sod	Hollow spheres	Zhou et al. (2020a) and Tan and Zeng (2016)
67	$Co(MeIM)_2$	Sod	Flower-like	Wang et al. (2019)

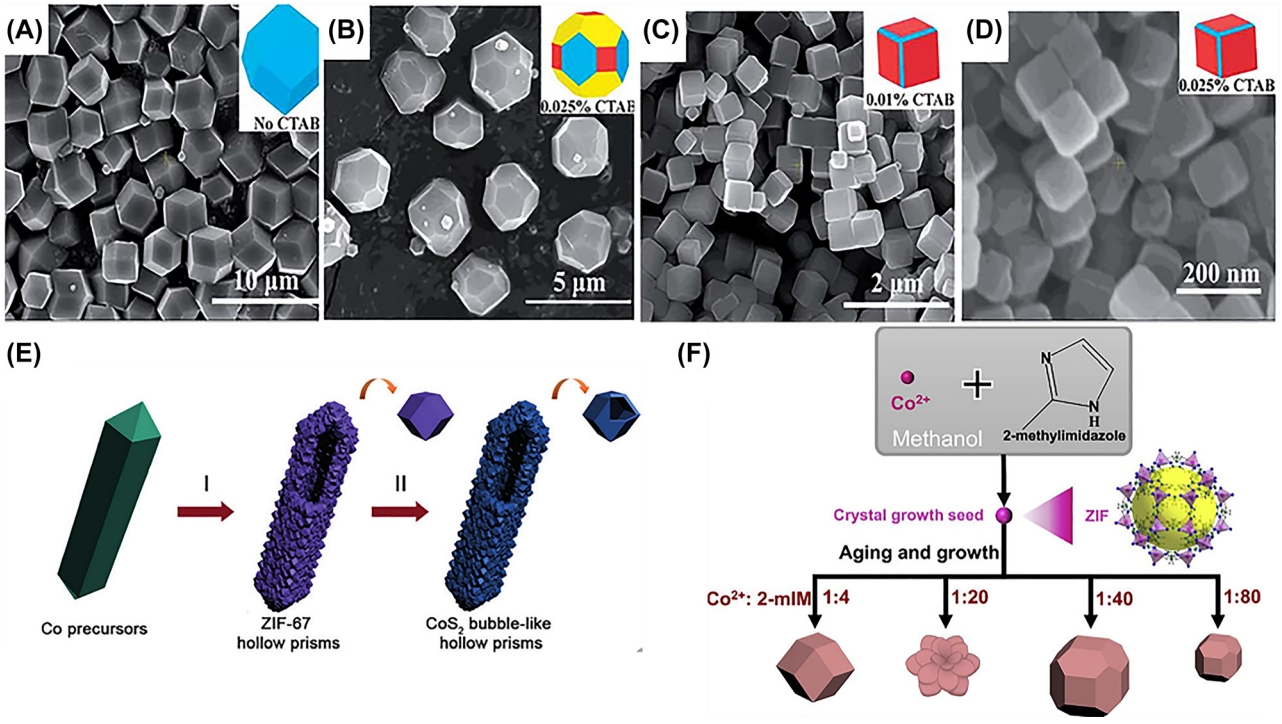

Figure 3: Images of ZIF-8 crystals. SEM images of (A) pure ZIF-8 crystal, (B) ZIF-8 crystal with 0.0025% CTAB, (C) ZIF-8 crystal with 0.01% CTAB, and (D) ZIF-8 crystal with 0.025% CTAB (Pan et al. 2011). (E) The schematic diagrams of preparation of ZIF-67 hollow prisms (Yu et al. 2016). (F) The synthesis and corresponding morphologies of ZIF-67 precursors (Wang et al. 2019). Copyright permission obtained to reproduce from RSC Publishing, STM Signatory Publisher and Elsevier.

uniform shell thickness can be obtained by the MOF-to-MOF conversion method in the 2-methylimidazole solution. The fabrication of the hollow ZIF-8 spheres is based on the structural features of MOF-5 (e.g., high porosity) and the stronger coordination bond between Zn^{2+} and 2-methylimidazole. Furthermore, the ZIF-8 with the cage-like morphology have also been synthesized as precursors to prepare the hierarchical porous ZnO nanocages for their excellent gas-sensing performance (Zhang et al. 2019d).

Lou et al. (2016) have synthesized the uniform ZIF-67 hollow prisms structure though the ion-exchange method directly converting cobalt acetate hydroxide into ZIF-67 in ethanol. Furthermore, the CoS_2 bubble-like hollow nanoparticles can be further constructed by ZIF-67 hollow prisms via a sulfidation reaction, then the CoS_2 nanobubble hollow prisms can be obtained from the conversion of CoS_2 bubble-like hollow nanoparticles under the annealing treatment (Figure 3E). Yu et al. (2015) reported that four novel kinds of ZIF-67 had been prepared through a simple and green method at room temperature by converting crystalline cobalt carbonate hydroxide. Importantly, the aqueous solution involved in this method without any toxic organic solvents. By particularly controlling some experimental conditions including reaction time and temperature, and the concentration of the solution, diverse morphologies of ZIF-67 can be obtained, such as core-shell nanowires, bead-on-string structure, nanotube, and nanoflake. Moreover, a series of ZIF-67 precursors with various shapes and sizes have also been synthesized for preparing their derivative porous metal oxides (Figure 3F) (Wang et al. 2019). These four morphologies of ZIF-67 were specially designed via the suitable ratios of Co^{2+} ions and 2-methylimidazole, which showed excellent shape-controllable features.

The pore size of ZIFs is also essential to optimize the performance of ZIFs and their derivatives. ZIFs inherit the structural characteristics of zeolites and MOFs with controllable pore size configuration and large surface areas, and are therefore promising candidates for gas storage and gas separation. Benefit from the unique pore structure characteristics, they exhibit significant sieving advantages in that gas with sizes larger than the pore size would be intercepted. For instance, the ZIF-8 membranes with a pore size of 0.34 nm are often recommended as a promising candidate for hydrogen (0.29 nm) separation from CO_2 (0.33 nm), N_2 (0.36 nm), and CH_4 (0.38 nm). Therefore, these ZIFs with controllable pore size and large surface area are often employed in gas sensing

applications to separate the interfering gases from the target gases and thus can greatly improve the selectivity and sensitivity of the gas sensors.

3 General properties and applications of ZIF-X (8, 67)

To this day, numerous porous materials have been explored as porous adsorbents or membranes for gas adsorption and separation, such as carbon nanotubes, activated carbon, zeolites, aluminophosphates, and silica gels. As an important class of crystalline porous materials, ZIFs are considered ideal candidates for gas storage and separation (Aceituno Melgar et al. 2015; Gong et al. 2017; Guan et al. 2020). Among various ZIFs materials, Zn-ZIF-8 and Co-ZIF-67 are the most representative materials, have been widely applied in gas adsorption applications by reason of their distinct structural features. Compared with other ZIF materials, ZIF-8 and ZIF-67 not only exhibit unexpected chemical stability but also show outstanding thermal stability, which is of great significance to their practical applications. For example, ZIF-67 can basically maintain the original crystal morphology at a high-temperature of 350 °C, and ZIF-8 can stable up to 500 °C (Park et al. 2006; Qian et al. 2012). In addition, ZIF-8 and ZIF-67 possess comparable chemical stability, and they can stable in poor conditions such as boiling water and some of the organic solvents (e.g., boiling methanol). Moreover, ZIF-8 and ZIF-67 share the same sod topology with sodalite zeolites. Both materials exhibit excellent structural features among ZIFs materials, and they possess a high surface area (e.g., 1821 m^2/g for ZIF-8,1888 m^2/g for ZIF-67) and high pore volumes (Zhou et al. 2017).

Over the years, various ZIFs materials have been applied as novel adsorbent materials for gas storage to meet the global energy and environmental challenges. Numerous studies have already demonstrated that the gas adsorption capacities of porous ZIFs have a strong correlation with their pore volumes or surface areas (Houndonougbo et al. 2013; Li et al. 2014a; Meng et al. 2020). Therefore, owing to the excellent structural characteristics including huge surface area and ordered porous structures, both ZIF-8 and ZIF-67 exhibit superior gas adsorption capacity (e.g., hydrogen storage, carbon dioxide capture, and methane storage). In 2017, Zhou et al. reported a comparative study on ZIF-X (8, 67) for the gas (CH_4, N_2, and CO_2) adsorption properties. In this work, compared with CH_4 and N_2 adsorbed gases, both ZIF-8 and ZIF-67 exhibit the largest adsorption capacity for CO_2. Therefore, ZIF-8 and ZIF-67 have also been regarded as promising materials for CO_2 adsorption. In addition, to obtain better CO_2 adsorption properties of ZIF-X (8, 67) based nanomaterials, various functionalization strategies have been developed. For instance, Tsai et al. (2018) reported that the organic linkers of ZIF-8 were successfully exchanged with several known imidazoles by solvent assisted ligand exchange method. The modified ZIF-8 has various functional groups, particles with SH functionalities exhibit a 2-fold improvement in CO_2 adsorption capacity compared with unexchanged ZIF-8. Moreover, Song et al. (2020) synthesized two series of ion-exchanged ZIF-67 (i.e., Li-ZIF67 and Na-ZIF-67) by a novel one-step ion-exchange strategy to improve CO_2 uptake performance. By comparison, the ion-exchanged ZIF-67 exhibits a higher CO_2 adsorption capacity, resulting from the enhanced electrostatic interaction caused by the ion-exchange method. Similarly, Akbari Beni and Niknam Shahrak (2020) have successfully designed three alkali-functionalized ZIF-8 nanostructures (i.e., Li, K, and Na) using density functional theory calculations in a molecular simulation study. The simulated CO_2 adsorption isotherms of functionalized ZIF-8 at 298 k from 0 to 150 kPa. The uptake capacity of pristine ZIF-8 was lower than that of alkali-functionalized ZIF-8. Furthermore, among the functionalized ZIF-8 structures, Li-ZIF-8 shows the highest CO_2 adsorption of 6 mmol/g. The higher storage performance in Li-ZIF-8 could be attributed to the enhanced interaction between Li-functionalized ZIF-8 and CO_2 molecules.

In 2014, Cheng and Hu (2014) prepared a stable H_2O-functionalized ZIF-8 via a simple and effective water treatment approach, which exhibits a significantly enhanced H_2 adsorption capacity at ambient temperature compared to pristine ZIF-8. Furthermore, Pt@ZIF-8/graphene oxide composites were synthesized through the simple liquid impregnation route, in which Pt nanoparticles act as the metal catalyst (Zhou et al. 2015). In this work, the hydrogen storage capacities of pure ZIF-8 and the as-synthesized composites were systematically investigated. Pt@ZIF-8/GO composite show the remarkably enhanced H_2 capacity at ambient temperature compared to ZIF-8 and ZIF-8/GO. Such improved H_2 capacity could be ascribed to the catalytic spillover mechanism. As mentioned above, ZIF-8 and ZIF-67 show great potential for gas storage applications and various functionalisation techniques (e.g., ion exchange, ligand functionalization, and inorganic substance-ZIF composites) have been developed to further improve gas adsorption capacity.

4 Gas-sensing applications

In recent years, due to the poor air quality caused by excessive exhaust emissions from factories, people are

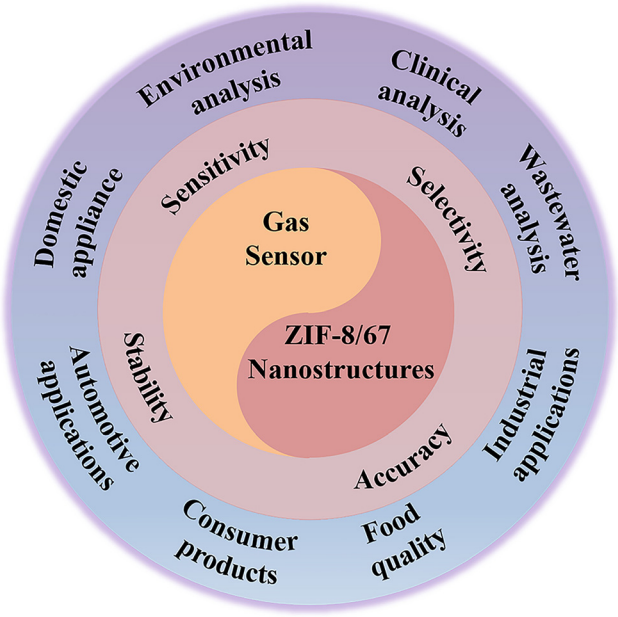

Figure 4: The important parameters and applications of gas sensors.

increasingly concerned about health problems. Therefore, the detection of toxic and harmful gases is urgently needed and thereby facilitate the solution of air pollution problems. More importantly, apart from the environmental analysis, high-performance gas sensors have also been applied in versatile fields, such as clinical analysis, wastewater analysis, industrial applications, food quality, consumer products, automobile, and domestic appliances (Figure 4) (Bhargav et al. 2014; Blanco-Rodriguez et al. 2018; Tai et al. 2020; Wales et al. 2015; Wojnowski et al. 2017). It is known that the key factor for the development of superior performance gas sensors is the high-performance sensing materials. With the rapid development of materials science, numerous novel types and structures of gas-sensing materials are continually emerging, which provides a promising opportunity for the development and application of gas sensors.

As a burgeoning novel class of porous material, ZIFs materials have attracted tremendous attention as gas-sensing materials, and extensive strategies have been developed to design various nanostructures of ZIFs materials to optimize their functionality and applications. In fact, various ZIF-X (8, 67) based nanostructures for gas-sensing applications have been intensively investigated due to the following attractive properties:(1) They possess distinct structural characteristics (such as tunable pore aperture enables them to serve as molecular sieves, which can significantly improve the selectivity of sensitive materials, high surface areas and ultra-porous nature ensure that they can provide sufficient adsorption sites for the target gas and oxygen molecules, which is of great benefit to the detection sensitivity). (2) Extremely high stability as traditional zeolites, and can maintain stability under some harsh environmental conditions, which can ensure a great long-term stability for sensing materials. (3) ZIF-8 and ZIF-67 are an emerging platform that can be easily functionalized (e.g., loaded metal nanoparticles), and the functionalized composites can then be used as templates for the preparation of their derivatives to enable the achievement of high-performance sensitive materials. As of today, numerous advanced nanostructures of ZIF-X (8, 67) and their derivatives have been designed to detect distinct toxic and harmful gases. In general, the same sensitive materials with different structures and morphologies would exhibit significantly different structural features such as different specific surface area, pore size, and surface active sites. All those structural parameters are the key factors in optimizing the gas-sensing performance. Therefore, the control of the morphology and nanostructure of ZIF-X (8, 67) is vital for optimizing the parameters of ZIF-X (8, 67) based sensors. Meanwhile, it is urgent to further explore the relationship between gas-sensing performance and structural features for superior gas-sensing performances. Various ZIF-X (8, 67) based gas sensors have been developed in previous reports, which can be divided into two categories: VOCs sensor (Table 2) and inorganic gas sensor (Table 3). (Wang et al. 2018b; Zhang et al. 2020a, 2020c, 2020e)

4.1 VOCs sensors

4.1.1 Acetone sensors

Acetone sensor as a critical class of VOCs sensors, various ZIF-X (8, 67) based nanostructures have been intensively investigated as gas sensing materials to enhance its sensitivity and selectivity. As a family of metal oxide semiconductors (MOSs), ZnO and Co_3O_4 have gained tremendous attention for gas sensing due to their fast response and relatively low cost. However, the traditional metal oxide based gas sensors commonly exhibit low selectivity and high operating temperature, which are great obstacles for their further application. To enhance the poor gas-sensing properties, numerous MOSs with unique nanostructures derived from ZIF-X (8, 67) materials have been explored for their ultra-high surface areas and abundant chemical active sites. It is believed that porous structures are one of the most popular nanostructures owing to their unique features. Therefore, numerous ZIF-X (8, 67) based gas-sensing materials with porous structures

Table 2: Summary of the sensing performances of ZIF-X (8, 67) based nanostructures gas-sensing applications for the detection of VOCs.

ZIF	Derivatives	Nanostructure	Analyte	Working temperature (°C)	Response [SG2]	Concentration (ppm)	t_{Res}/t_{Rec} (s)	LOD (ppm)	References
ZIF-8/ZIF-67	ZnO/Co_3O_4	Porous	Acetone	275	15.17	1	317/390	–	Xiao et al. (2018)
Au/ZIF-8	Au/ZnO	Porous	Acetone	275	17.1	1	231/215	0.1	Xia et al. (2017)
ZIF-67	Au/Co_3O_4	Porous cubic	Acetone	220	22.19	100	27/70	10	Cui et al. (2019)
ZIF-67	Co_3O_4/FGH	Porous	Acetone	250	81.2	50	20	1	Ding et al. (2018)
ZIF-8	ZnO/S,N: GQDs/PANI	Porous	Acetone	RT	2	0.5	15/27	0.1	Zhang et al. (2019a)
ZIF-8/ZIF-67	ZnO/Co_3O_4	Hollow	Acetone	300	30.1	100	8/2	1	Zhang et al. (2019)
ZIF-67/Co-Zn LDH	$Co_3O_4/ZnCo_2O_4$	Hollow	Acetone	255	16.3	100	41/47	0.51	Qu et al. (2018)
ZIF-67	Co_3O_4/Fe_2O_3	Hollow cubes	Acetone	250	3.27	100	–	–	Xu et al. (2020a)
Pd-ZIF-67	Co_3O_4/PdO/n-SnO_2	Hollow nanocubes	Acetone	450	22.8	5	90.8/108.4	0.005	Jang et al. (2017)
Pd@ZIF-8	PdO@ZnO–SnO_2	Hollow nanotubes	Acetone	400	5.06	1	20/64	0.01	Koo et al. (2017a)
Pd-ZIF-67	PdO-Co_3O_4	Hollow nanocages	Acetone	350	2.51	5	–	0.1	Koo et al. (2017b)
ZIF-67/Ni–Co LDH	$Co_3O_4/NiCo_2O_4$	Double-shelled nanocages	Acetone	238.9	3.09	100	8/20	–	Qu et al. (2017a)
ZIF-67	Co_3O_4	Core–shell	Acetone	190	13	200	4/8	–	Zhang et al. (2018a)
ZIF-8	ZnO@MoS_2	Nanosheets core/shell	Acetone	350	150	0.5	9/17	0.005	Chang et al. (2020)
Au-ZnO@ZIF-8	–	Nanowire array	Acetone	275	231	100	~180/~60	0.0034	Yao et al. (2019)
ZnO@ZIF-8	–	Hollow nanofibers	Acetone	263	60	100	–	2	Tian et al. (2020)
ZIF-8/ZIF-67	–	Hexagonal shapes	Ethanol	180	–	90	390/348	10	Matatagui et al. (2018)
ZIF-67	Co_3O_4	Porous concave nanocubes	Ethanol	300	–	200	<10	10	Lu et al. (2014)
ZIF-67	Co_3O_4	Porous hollow	Ethanol	200	221.99	100	129/216	1	Zhang et al. (2020b)
ZIF-67	ZnO–Co_3O_4	Nanofibers	Ethanol	200	106	1000	7/236	1	Xiong et al. (2017)
ZIF-67	TiO_2/Co_3O_4	Porous polyhedral	Ethanol	150	16.7	150	–	5	Zhang et al. (2018b)
ZIF-8	ZnO	Hollow nanocages	Ethanol	325	139.41	100	2.8/56.4	0.025	Zhang et al. (2019d)
Ag–ZIF-8	Ag–ZnO	Hollow nanocages	Ethanol	250	84.6	100	5/10	0.0231	Zhang et al. (2019)
ZIF-8	Fe_2O_3/ZnO/Au	Hexagonal-like	Ethanol	280	170	100	4/5	10	Chen et al. (2018)
ZIF-8	CNT@$ZnSnO_3$	Hollow boxes	Ethanol	240	166	100	6	1	Guo et al. (2020)
ZIF-8@ZnO	ZnO	Neck-connected ZnO films	Ethanol	375	124 (I_g/I_a)	50	120/70	0.5	Qi et al. (2019)
ZnO@ZIF-8	–	Core–shell	Ethanol	160	35.9	100	23/31	–	Ren et al. (2019)
ZIF-67	–	Porous	Formaldehyde	150	13.9	100	–	5	Chen et al. (2014)
ZIF-8	–	Porous	Formaldehyde	RT	6.25	100	94/79	–	Reddy et al. (2020)
ZnO@ZIF-8	–	Core–shell	Formaldehyde	300	–	100	16/9	5.6	Tian et al. (2015)
POM@ZIF-8@ZnO	–	Core–shell	Formaldehyde	25	–	100	15.1/16.2	0.387	Wang et al. (2018a)

Table 2: (continued)

ZIF	Derivatives	Nanostructure	Analyte	Working temperature (°C)	Response [SG2]	Concentration (ppm)	t_{Res}/t_{Rec} (s)	LOD (ppm)	References
ZIF-67/Co–Fe	$Co_3O_4/CoFe_2O_4$	Double-shelled nanocubes	Formaldehyde	139	12.7	10	4/9	0.3	Zhang et al. (2019b)
ZIF-8/Co-Zn hydroxide	$ZnO/ZnCo_2O_4$	Hollow core–shell nanocages	Xylene	320	34.26	100	–	0.126	Qu et al. (2016)
ZIF-8/Ni-Zn LDH	$ZnO/Ni_{0.9}Zn_{0.1}O$	Double-shelled nanocages	Xylene	240	54.7	100	–	0.12	Qu et al. (2017b)
Ti loaded ZIF-67	Co_3O_4/TiO_2	Rhombic dodecahedron	Xylene	120	6.17	50	<23	8.6	Bai et al. (2018)
ZIF-67	Co_3O_4	Hollow nanocages	Xylene	225	78.6	5	63/86	0.25	Jo et al. (2018)
Pd@ZIF-8	Pd@ZnO–WO_3	Nanofibers	Toluene	350	22.22	1	20	0.1	Koo et al. (2016)
ZIF-8/ZIF-67	–	Hexagonal shapes	Toluene	180	–	90	150/186	10	Matatagui et al. (2018)
ZIF-67	Co_3O_4	Porous	n-Butanol	100	21	100	146/90	5	Wang, et al. (2019)
ZIF-8	ZnO	Clusters	n-Butanol	300	37.8	10	10	0.1	Zhang et al. (2019c)
SnS_2/ZIF-8	SnO_2/ZnO	Porous flower-like	Triethylamine	200	17.7	50	9/10	–	Ma et al. (2019)
ZIF-8@ZIF-67	Co_3O_4/ZnO	Co_3O_4 quantum dots/ZnO nanocages	Trimethylamine	190	232	50	2.1/11.8	0.013	Li et al. (2020b)
ZIF-8	ZnO	Hierarchical hollow cubes	Benzene	400	(1.21)	0.1	76 ± 16/ 82 ± 17	0.1	Li et al. (2015)

Table 3: Summary of the sensing performances of ZIF-X (8, 67) based nanostructures gas-sensing applications for the detection of inorganic gas.

ZIF	Derivatives	Nanostructure	Analyte	Working temperature (°C)	Response [SG3]	Concentration (ppm)	t_{Res}/t_{Rec} (s)	LOD (ppm)	References
ZIF-8/ZIF-67	–	Hexagonal shapes	H_2	180	–	90	132/186	10	Matatagui et al. (2018)
ZnO@ZIF-8	–	Core-shell nanorods	H_2	250	3.28	50	–	–	Wu et al. (2017)
ZnO@ZIF-8	–	Core-shell nanorods	H_2	275	–	50	50/130	–	Khudiar et al. (2020)
ZnO@ZIF-8	–	Core-shell microrods	H_2	125	8.61	50	100/20	0.5	Cui et al. (2018)
ZnO@ZIF-8	–	Core-shell nanowires	H_2	300	1.44	50	–	–	Drobek et al. (2016)
ZIF-8/Pd/ZnO	–	Core-shell nanowires	H_2	200	8.5 ± 0.4	50	–	–	Weber et al. (2018)
ZIF-8@ZnO	–	Core-shell nanowires	H_2	250	72.3	100	–	–	Jeon et al. (2020)
ZIF-67	PdO–Co_3O_4	Nanocubes	NO_2	100	44.11	20	–	1	Choi et al. (2017)
ZIF-67	MWCNTs	Nanocubes	NO_2	RT	1	5	–	0.1	Rui et al. (2018)
WS_4_ZIF-67	WS_2_Co–N–HCNC	Hollow nanocages	NO_2	RT	48.2	5	–	0.1	Koo et al. (2018)
ZnCo-ZIF	–	Nanosheets	NO_2	RT	54.6	100	1.01/12	0.01	He et al. (2021)
ZIF-8/ZIF-67	–	Hexagonal shapes	NO_2	180	–	90	348/330	10	Matatagui et al. (2018)
In_2O_3/ZIF-8	–	Core-shell In_2O_3 nanofibers	NO_2	140	16.4	1	80/133	0.01	Liu et al. (2019)
ZIF-8@ZnO	–	Nanowires	NO_2	250	60.6	20	–	–	Jeon et al. (2020)
ZIF-8/ZnO	–	Nanorod	H_2S	25	52.1	10	420/-	0.05	Wu et al. (2019b)
Pt@ZIF-8	Pt/ZnO	Three-dimensional macroporous	H_2S	320	11.2	1	8.7/19.4	0.025	Zhou et al. (2020b)
ZIF-67/Ni–Co	Co_3O_4/$NiCo_2O_4$	Double-shelled nanocages	H_2S	250	57	50	153/40	–	Tan et al. (2020)
ZIF-8/ZIF-67	–	Hexagonal shapes	CO	180	–	90	456/264	10	Matatagui et al. (2018)
ZIF-67	Co_3O_4	Porous	CO	150	220	100	–	0.5	Qin et al. (2020)
SnO_2@ZIF-67	–	Core–shell	CO_2	205	16.5	5000	96/25	5000	Me et al. (2018)
ZIF-8	–	Porous	NH_3	RT	1.33	10	63/45	–	Reddy et al. (2020)
ZIF-8@ZnO	–	Nanowires	NH_3	250	77.7	10	–	0.5	Jeon et al. (2020)
Zinc doped ZIF-67	CoZn-NCNTs	Porous polyhedral	SO_2	RT	28.9	30	–	30	Li et al. (2018a)

have been designed to enable excellent sensing performance. For example, the porous ZnO/Co_3O_4 nanomaterials derived from ZIF-X (8, 67) can detect ppb to ppm level of acetone at 275 °C, and exhibited a notable response of 15.17 towards 1000 ppb of concentration (Xiao et al. 2018). Moreover, to further improve gas-sensing performance, the introduction of noble metals (e.g., Au) into porous nanostructures is considered as a promising method. Xia et al. (2017) synthesized porous Au/ZnO nanocomposites by direct pyrolysis of Au/ZIF-8 nanoparticles. The as-synthesized porous Au/ZnO nanocomposites at 275 °C performed obviously enhanced response and acetone selectivity at low concentration. For example, the gas-sensing sensitivity of Au/ZnO (17.1) nanocomposites is higher than the porous ZnO nanoparticles (7.9) towards 1000 ppb of acetone. Meanwhile, they also constructed porous Au/Co_3O_4 microstructures using the same strategy described above (Cui et al. 2019). The as-synthesized

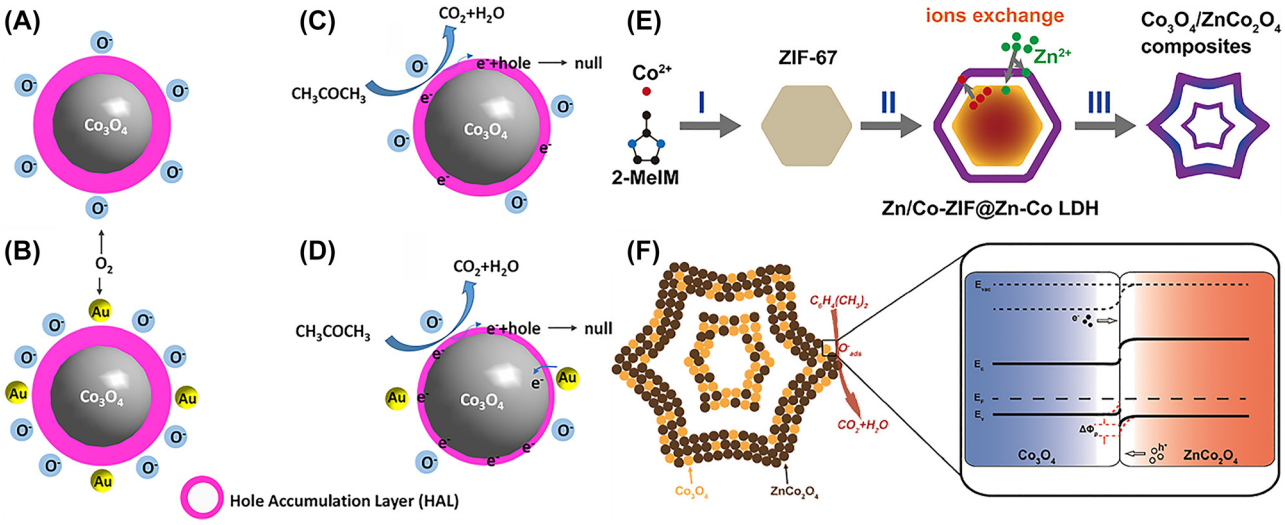

Figure 5: Sensing mechanism of Au/Co_3O_4 nanocomposites. (A–D) The sensing mechanism of Au/Co_3O_4 nanocomposites (Cui et al. 2019). (E) The preparation process of $Co_3O_4/ZnCo_2O_4$ nanostructure using ZIF-67 as precursor, and f the acetone sensing mechanism (Qu et al. 2018). Copyright permission obtained to reproduce from Elsevier.

porous Au/Co_3O_4 samples retained a similar morphology to the ZIF-67 template and greatly improved its pore structure. Therefore, combining the structural characteristics of Co_3O_4 and the catalysis of Au, the porous Au/Co_3O_4 composites as acetone-sensing materials exhibits higher gas-sensing performance than pure Co_3O_4. The porous Au/Co_3O_4 composites performed obviously improved acetone response (R_g/R_a = 21.95) compared to singular Co_3O_4 nanoparticles (R_g/R_a = 11.35) toward 100 ppm acetone. In addition, the porous Au/Co_3O_4 composites exhibited a shorter response-recovery time toward acetone gas. The two works above demonstrated that the Au/ZnO and Au/Co_3O_4 exhibited enhanced sensing performance can be attributed to the unique porous structure, the spillover effect of Au nanoparticles, and its catalytic and electronic activities (Figure 5A–D). Meanwhile, these results might provide a novel way for the design of porous noble metal/semiconductor metal oxide composites for development of high performance gas sensors.

Ding et al. (2018) fabricated porous Co_3O_4/FGH composites from the precursor ZIF-67/functionalized graphene oxide hydrogels (FGH) composites. Take advantage of unique porous nanostructures and optimization of electrical properties of composite materials with the chemically functionalized FGH, the porous Co_3O_4/FGH composites showed a markedly high acetone response (R_{gas}/R_0 = 81.2@ 50 ppm), which was ~20-fold higher compared with pure Co_3O_4 film. Furthermore, the porous Co_3O_4/FGH composites exhibited rapid response time (within 20 s) and excellent selectivity to acetone gas. In addition, Zhang et al. (2019a) reported the ZnO/S, N: GQDs/PANI (GQDs = graphene quantum dots, PANI = polyaniline) nanocomposites synthesized through *in-situ* polymerization strategy. The sensor based on ZnO/S, N: GQDs/PANI nanocomposites exhibited ppb-level sensitivity, remarkable acetone selectivity, excellent long-term stability, and rapid response/recovery speed towards acetone at room temperature. Meanwhile, the effect of humidity on the gas sensing performances of the gas sensor is negligible, making it appropriate for the detection of exhaled acetone gas.

Recently, hollow nanomaterials have been extensively designed as high-performance gas sensing materials because of their remarkable structural characteristics (e.g., high specific surface area and low densities). For example, using the ZIF-8/ZIF-67 mixture as the self-sacrificing template, Zhang et al. (2019b) fabricated hollow ZnO/Co_3O_4 heterostructures nanocomposite. The use of as-synthesized ZnO/Co_3O_4 hollow nanostructure samples as acetone sensing materials shows a significantly enhanced sensing performance (e.g., superior response, remarkable selectivity, outstanding repeatability, and excellent linearity) compared with pristine ZnO. Similarly, hollow nanostructure $Co_3O_4/ZnCo_2O_4$ composites have also been developed via a self-templating strategy (Figure 5E) (Qu et al. 2018). This strategy includes three steps, the ZIF-67 template was first synthesized and then transformed into Co/Zn-ZIF@Co-Zn layered double hydroxide (LDH) precursor. Finally, hollow $Co_3O_4/ZnCo_2O_4$ composites were prepared through calcination of as-prepared Co/Zn-ZIF@Co-Zn LDH precursor. The as-prepared hollow nanostructure $Co_3O_4/ZnCo_2O_4$ composites showed enhanced gas sensing performance compared with hollow $ZnCo_2O_4$ and Co_3O_4. The acetone

sensing properties of $Co_3O_4/ZnCo_2O_4$ heterojunctions nanostructures are strongly affected by the surface adsorbed oxygen species, and the acetone sensing mechanism shown in Figure 5F. Once acetone gas is injected, the acetone gas would react with the adsorbed oxygen ions, and then release the trapped electrons back to Co_3O_4 and $ZnCo_2O_4$, and the reaction can be described by Eq. (1): $CH_3COCH_3ads + 8O^-ads \rightarrow 3CO_2 + 3H_2O + 8e^-$). And the constructed heterojunctions nanostructures can provide more active sites for adsorption of oxygen and acetone molecules; therefore, the construction of heterojunctions is one of the important factors the enhancement of sensing properties. Furthermore, the excellent sensing properties are also attributable to the porous structure and the formation of thin shells.

Xu et al. (2020) synthesized hollow Co_3O_4/Fe_2O_3 nanocubes through the MOF hybrid-assisted method. The as-synthesized hollow Co_3O_4/Fe_2O_3 nanocubes exhibited 3.06-fold higher response value (R_g/R_a = 3.27) to acetone gas than that of Co_3O_4 nanocubes, which could be attributed to unique hollow porous structures and the formation of p–n heterojunctions.

In 2017, The group of Kim (Jang et al. 2017; Koo et al. 2017a; Koo et al. 2017b) reported three catalyst functionalized acetone-sensing materials with hollow structures. The first one, Co_3O_4–PdO loaded n–SnO_2 hollow nanocubes (HNCs) were prepared via galvanic replacement reaction (GRR), in which ultra small PdO nanoparticles and Co_3O_4 island as cocatalysts to functionalize n–SnO_2 (Figure 6A) (Jang et al. 2017). The GRR-treated SnO_2 showed significantly enhanced gas sensing performance compared with hollow p-type Co_3O_4 derived from ZIF-67. For example, the n–SnO_2–Co_3O_4–PdO HNCs showed 21.9 times higher response (R_{air}/R_{gas} = 22.8–5 ppm) toward acetone compared with hollow p-type Co_3O_4. Meanwhile, this group also prepared the PdO@ZnO–SnO_2 nanotubes through the electrospinning and followed calcination (Koo et al. 2017a). The nanoscale PdO catalysts (3–4 nm) and heterojunction structures (ZnO–SnO_2 and PdO–ZnO) were effectively loaded on the surface of Co_3O_4 HNCs. Benefiting from the advantages of the unique hollow nanotube structures, PdO@ZnO–SnO_2 NTs can exhibit high specific surface areas and considerable open porosity. Therefore, the PdO@ZnO–SnO_2 NTs as acetone gas sensing materials showed a superior response (R_{air}/R_{gas} = 5.06 to 1 ppm at 400 °C), excellent acetone selectivity, and rapid response/recovery speed (20/64 s) at substantially humid conditions (95% RH). Kim et al. (2017) also reported that ultrasmall Pd catalyst well-dispersed Co_3O_4 hollow nanocages (HNCs) derived from ZIF-67 templates were good candidates as acetone gas sensor. With the unique structure of Co_3O_4 HNCs and functionalization of PdO NPs, the PdO–Co_3O_4 HNCs showed a markedly enhanced response (R_g/R_a = 2.51@5 ppm acetone at 350 °C) compared to Co_3O_4 NPs (1.45), Co_3O_4 HNCs (1.96), and PdO–Co_3O_4 NPs (1.98). Moreover, the PdO–Co_3O_4 HNCs exhibited outstanding selectivity toward acetone gas.

Qu et al. (2017a) reported $Co_3O_4/NiCo_2O_4$ double-shelled nanocages (DSNCs) obtained by thermal treatment of ZIF-67/Ni-Co LDH precursor in air. When used as a gas sensing material, the obtained $Co_3O_4/NiCo_2O_4$ DSNCs give an improved sensitivity, outstanding reversibility, and excellent selectivity toward acetone gas compared to Co_3O_4 NCs. Zhang et al. (2018a) have successfully prepared four novel porous Co_3O_4 hierarchical structures by controlling the calcination environment (i.e., atmosphere, temperature, and calcination rate) from ZIF-67 templates. Take the advantages of core–shell hierarchical structure, both core–shell Co_3O_4 sample and porous core–shell Co_3O_4 sample performed a higher response value (i.e., 13 and 11, respectively) toward acetone gas at 190 °C than the response values of porous popcorn and nanoparticle structures (i.e., 7.9 and 2.6, respectively). In addition, both core–shell and porous core–shell Co_3O_4 samples exhibited short response/recovery time (share the same values of 4/8 s) toward acetone gas, which is far shorter than the values of porous popcorn and nanoparticle structures.

More recently, Chang et al. (2020) reported the highest response value toward acetone gas among ZIF-X (8, 67)-based sensing materials. In their report, ZIF-8 was used as a precursor to obtaining ZnO, and then the core/shell ZnO@MoS_2 nanosheets heterojunctions were prepared via a facile hydrothermal method. The ZnO@MoS_2 heterogeneous nanostructures exhibited ~80-fold improvement of response value than that of singular ZnO toward 100 ppb of acetone at 350 °C (Figure 6B). Notably, the as-prepared ZnO@MoS_2 gave a super-rapid response time (60 s)/recovery time (40 s) toward super-low acetone gas concentration of 5 ppb, excellent acetone selectivity, and a negligible influence of humidity on the gas sensing performance (Figure 6C). To provide an in-depth understanding of the sensing mechanism of MoS_2, they calculated the interaction energy and charge transfer between various gas molecules and the MoS_2 surface by density functional theory (DFT) calculations, as shown in Figure 6(D–K). It is clear from the results of the DFT calculations that there is a stronger interaction between acetone and MoS_2 compared to other gases, which can be used to explain the excellent sensitivity and selectivity of ZnO@MoS_2 sensor towards acetone.

As discussed above, ZIF-based membranes have been extensively applied in gas storage and separation due to their outstanding structural features for gas adsorption and filtration. Thus, combining MOSs with the excellent

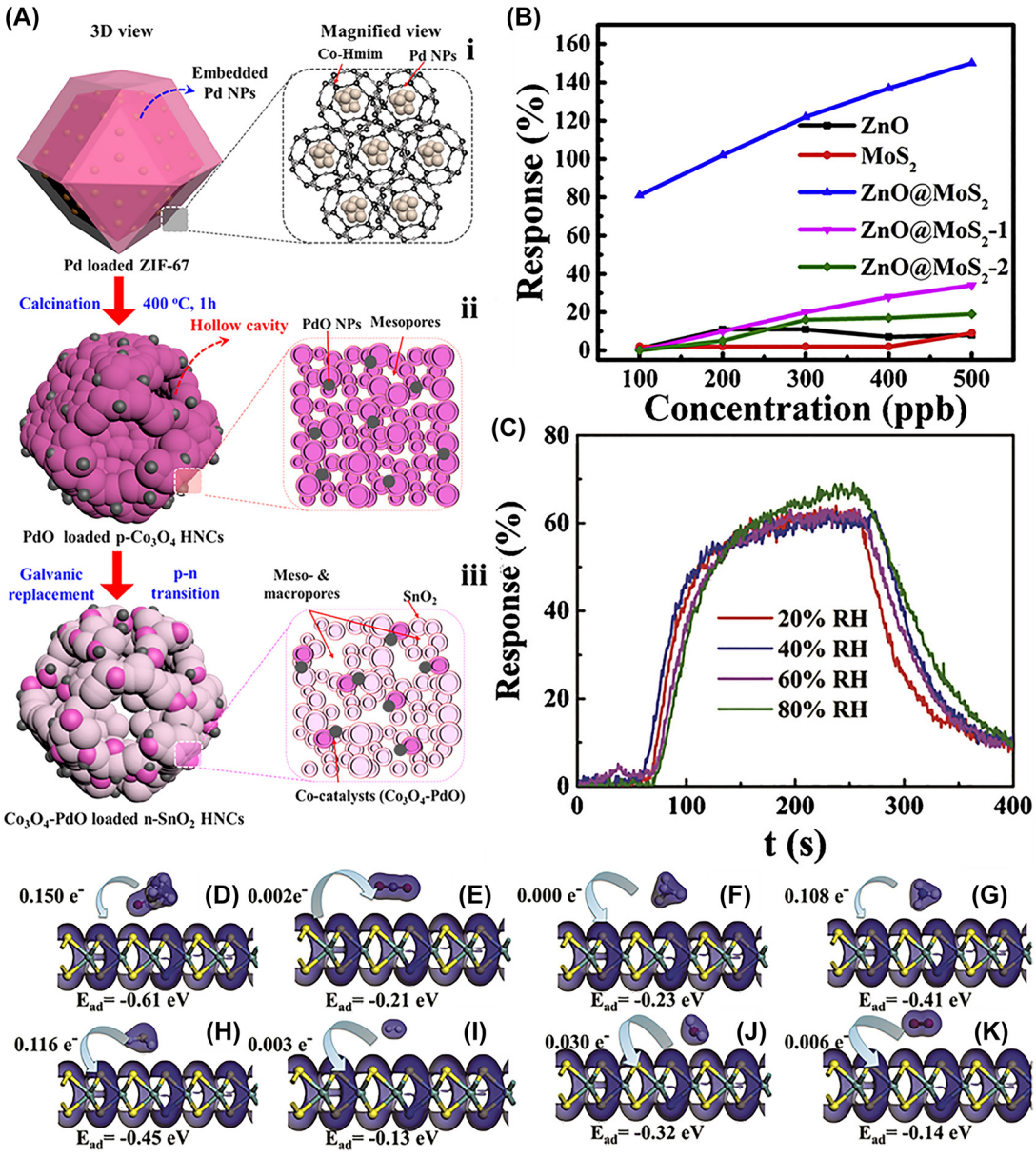

Figure 6: PdO loaded Co_3O_4–SnO_2 for acetone sensing. (A) The formation of PdO loaded Co_3O_4–SnO_2 from Pd loaded ZIF-67 precursor (Jang et al. 2017). (B) The acetone-sensing performances of ZnO@MoS_2 core/shell nanostructures at 350 °C (Chang et al. 2020). (C) Response of ZnO@MoS_2 core/shell nanostructures toward 100 ppb acetone under different RH. The charge transfer and interaction energy between acetone (D), CO_2 (E), CH_4 (F), NH_3 (G), H_2S (H), H_2 (I), H_2O (J), O_2 (K) and MoS_2 (Chang et al. 2020). Copyright permission obtained to reproduce from American Chemical Society and Elsevier.

selectivity of ZIFs together is also considered as a promising design strategy to improve the sensing performance of MOSs. For example, to further improve the MOSs selectivity to the analytic gases with similar sensing activity, Yao et al. (2019) developed a novel Au-ZnO@ZIF-8-Dimethylbenzimidazole (DMBIM) core-shell nanowires array with different thick ZIF-8 thin film (5, 30 and 50 nm). The as-prepared MO@MOF 5 nm-DMBIM exhibited the best acetone selectivity over benzene compared to all reported materials. Meanwhile, the as-prepared nanomaterials performed excellent sensitivity, remarkable long-term stability and rapid response/recovery speed. Similarly, Tian et al. (2020) developed unique ZnO@ZIF-8 hollow nanofibers to pursue superior sensing properties of ZnO-based chemoresistive sensor. Benefits from porous ZIF-8 thin layer and ZnO hollow nanofibers, the as-synthesized hollow ZnO@ZIF-8 showed remarkably enhanced sensitivity and selectivity to acetone gas compared with pure ZnO. The

obtained material can also detect acetone gas at 263 °C and maintain relatively stable under humid atmosphere (15–60% RH). Overall, the above described novel ZIF-X (8, 67) based nanostructures acetone gas sensors including their derivatives (e.g., metal oxide, noble metal-metal oxide, metal oxide composites) and ZIF/metal oxide composites exhibit superior acetone gas sensing properties, which not only develops several excellent acetone sensors for detection of exhaled breath, but also presents various novel and efficient ways for preparing high performance sensing materials.

4.1.2 Ethanol sensors

The ethanol sensing performance of porous Co_3O_4 concave nanocubes derived from ZIF-67 was reported by Lu et al. (2014). In this work, porous Co_3O_4 nanomaterial was prepared by a two-step strategy, the ZIF-67 concave nanocubes were first synthesized as self-sacrificial templates and then calcining the as-synthesized ZIF-67 templates at 300 °C (Figure 7A). They also systematically investigated the influence of calcination condition (i.e., calcination temperature) on the formation mechanism of specific morphologies and ethanol gas sensing properties. Benefiting from the significantly high surface area of 120.9 m^2/g that can absorb more oxygen species, the as-prepared Co_3O_4 concave nanocubes performed excellent selectivity, good sensing reproducibility, and high sensitivity with rapid response/recovery speed (less than 10 s). In addition, Zhang et al. (2020c) synthesized porous Co_3O_4 polyhedral nanostructures derived from the ZIF-67 sacrificial template, which showed the highest sensitivity to ethanol vapor compared to other reported Co_3O_4 materials. Apart from the high response, the porous Co_3O_4 sensors possess remarkable selectivity, excellent repeatability, and low operating temperature of 200 °C.

Xiong et al. (2017) synthesized porous ZnO–Co_3O_4 hollow polyhedron with p–n heterojunction nanostructure via a morphology-inherited thermal treatment of ZIF-67 precursor at 300 °C. The as-synthesized ZnO–Co_3O_4 heterostructure exhibited excellent performances to 1000 ppm of ethanol gas included high response value (106), applausive selectivity, and fast response/recovery speed (7/236 s) in comparison with pure porous Co_3O_4 nanomaterials, which can be explained by the formation of heterostructure and the porous hollow polyhedron structure. Additionally, the necklace-like TiO_2/Co_3O_4 nanofibers heterostructures were also successfully prepared through an electrospinning method and subsequent calcination

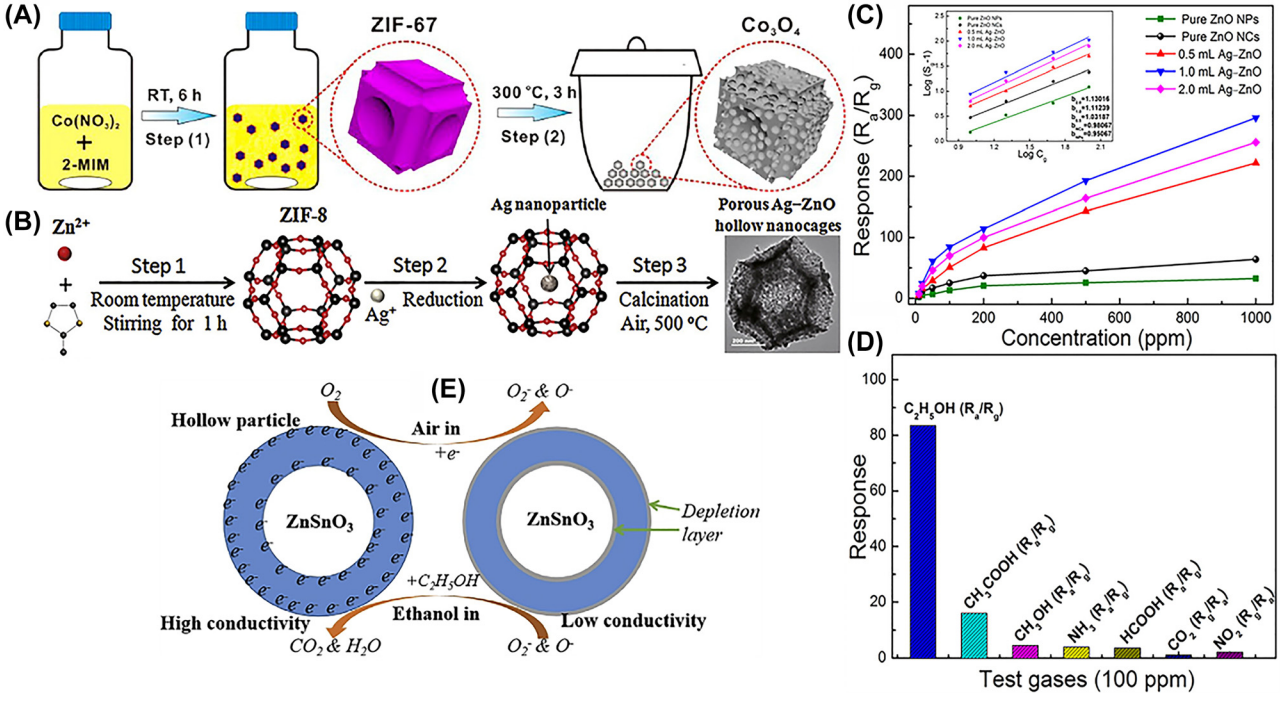

Figure 7: Hollow structures and gas sensing properties. (A) The fabrication of Co_3O_4 concave nanocubes by pyrolysis of ZIF-67 precursor Lu et al. (2014). (B) The synthesis procedure of Ag@ZnO hollow nanocages. (C) Responses of various ZnO nanostructures versus ethanol concentrations (10–1000 ppm) at 250 °C. (D) Sensing characteristics of Ag–ZnO hollow nanocages to various analytes at 250 °C. (E) The sensing mechanism to ethanol for CNT@$ZnSnO_3$ hollow structures (Guo et al. 2020). Copyright permission obtained to reproduce from American Chemical Society and Elsevier.

treatment. Similarly, taking the advantages of the excellent catalytic activity of Co_3O_4, the formation of heterojunctions, and the unique hierarchical structures, the TiO_2/Co_3O_4 heterostructures sensor presented a high ethanol response value of 16.7–150 ppm ethanol at 150 °C. Zhang et al. (2019g) constructed hierarchical ZnO-QD (quantum dots) hollow nanocages (HNCs) by direct pyrolysis of ZIF-8 templates at 390 °C for 50 min. Applied as sensing material, the obtained ZnO-QD (HNCs) exhibited ultra-high ethanol response (R_a/R_g = 139.41–100 ppm) at the working temperature of 325 °C and the response/recovery speed (2.8/56.4 s). Moreover, the as-prepared material can present a notable response value of 5.1 upon an ultra-low concentration of ethanol (<25 ppb). Such remarkable sensing performance benefits from the high specific surface area caused by quantum dots and the hierarchical hollow nanocages structure.

Furthermore, the Ag@ZnO HNCs were prepared via a MOF-based route, in which the nanoscale Ag with the size of 10 nm as catalysts to functionalize ZnO hollow nanocages (Figure 7B). The functionalized ZnO HNCs exhibited significantly enhanced response (84.6@100 ppm) toward ethanol and decreased working temperature of 250 °C compared to pure ZnO NCs and ZnO NPs (Figure 7C). Besides, the Ag@ZnO HNCs showed short response/recovery (5/10 s), remarkable response reproducibility, and excellent selectivity (Figure 7D). Such enhanced sensing performances could come from the catalytic effect of Ag NPs, porous hollow nanostructure, and larger surface area. Work by Chen et al. (2018) compared the sensing performance of α-Fe_2O_3/ZnO/Au nanocomposites, α-Fe_2O_3/ZnO heterostructures and α-Fe_2O_3 nanoplates to ethanol. Correspondingly, the α-Fe_2O_3/ZnO/Au nanocomposites display the largest BET surface area among the three materials (79.08 m^2/g for α-Fe_2O_3/ZnO/Au, 61.27 m^2/g for α-Fe_2O_3/ZnO, and 37.94 m^2/g for α-Fe_2O_3). Used as sensing materials, the as-prepared α-Fe_2O_3/ZnO/Au heterostructures showed outstanding ethanol sensing performances owing to the unique heterostructure, high surface area, the well-dispersed Ag NPs, and the synergistic effects of phase compositions. For instance, the α-Fe_2O_3/ZnO/Au nanocomposites exhibited a high response (170@100 ppm ethanol) at 280 °C, outstanding recycling stability, and fast response/recovery (4/5 s). More recently, Guo et al. (2020) reported a chemical sensor based on CNTs based perovskite type $ZnSnO_3$ fabricated by a facile hydrothermal reaction, where ZIF-8 used as Zn^{2+} source. The obtained CNT@$ZnSnO_3$ nanostructures featured a unique hierarchical structure with an exceptionally high surface area of 45.73 m^2/g, which is dramatically higher compared with solid $ZnSnO_3$ cube and hollow boxes $ZnSnO_3$ (6.53 and 28.41 m^2/g respectively). Thus, the chemical sensor was highly sensitive to ethanol (R_{air}/R_{gas} = 166–100 ppm) at 240 °C. The schematic illustration of ethanol sensing mechanism for CNT@$ZnSnO_3$ hollow structures is illustrated in Figure 7E. When the CNT@$ZnSnO_3$ hollow structure is exposed to ambient atmosphere, the O^- and O^{2-} will be produced through the reaction between O_2 molecules and electrons of $ZnSnO_3$, thus forming a thick electron-depleted layer. Upon exposure to ethanol gas, the formed O^- and O^{2-} can react with target gas molecules and release electrons back to CNT@$ZnSnO_3$ hollow structures, resulting in a low resistance value of CNT@$ZnSnO_3$ sensor.

In addition, it exhibited excellent ethanol selectivity, fast response time (6 s), and long-term stability. In addition, sensors based on neck-connected ZnO films exhibited dramatically enhanced sensitivity to ethanol (Qi et al. 2019). In this work, core-shell ZIF-8@ZnO films were used as precursors, and then the neck-connected ZnO films obtained by annealing treatment of the as-synthesized core-shell ZIF-8@ZnO films. The neck-connected ZnO films achieved markedly enhanced ethanol response value (I_g/I_a = 124–50 ppm), which increased by ~six times compared with ZnO film. Meanwhile, Ren et al. (2019) fabricated core-shell ZnO@ZIF-8 microspheres via a self-template method. In contrast with pristine hollow ZnO hollow microspheres, the core-shell ZnO@ZIF-8 microspheres exhibited significantly improved sensing properties towards ethanol, such as high response (35.90@100 ppm ethanol) and excellent selectivity to ethanol. The improved ethanol sensing properties were attributed to the enrichment effect of the uniform ZIF-8 shell.

4.1.3 Formaldehyde sensors

Chen et al. (2014) reported the gas sensing performance of pure MOFs ZIF-67 for the first time. Benefiting from the large surface area (1832.2 m^2/g) and remarkable stability, ZIF-67 exhibited high sensitivity and excellent selectivity at 150 °C to formaldehyde as gas sensor. It is worth noting that the ZIF-67 sensor can sense a low concentration of 5 ppm formaldehyde with a particular response value of 1.8. Additionally, the highly humid atmosphere (less than 70% RH) has a negligible effect on the formaldehyde sensing properties. These results demonstrated that porous pure MOFs ZIF-67 could be a promising gas-sensing material. Another pure MOF (ZIF-8) has also been investigated as sensing material for the formaldehyde gas sensor (Reddy et al. 2020). The ZIF-8 exhibited a low response value of 6.25–100 ppm formaldehyde. In 2015, Tian et al. fabricated core–shell ZnO@ZIF-8 nanorods via a self-template strategy, in which ZnO nanorods serve as the self-template and the source of

Zn^{2+} ions for synthesis of ZIF-8. The as-fabricated ZnO@ZIF-8 nanorods heterostructures showed significantly improved formaldehyde selectivity compared to the ZnO nanorods sensor, which was mainly attributed to the role of the ZIF–8 shell. Meanwhile, the response/recovery speeds were increased owing to the barriers of ZIF-8 shell. Likewise, Wang et al. (2018) reported the core-shell polyoxometalate@ZIF-8@ZnO nanocomposite for enhancing the formaldehyde sensing performances. Take advantage of the structural features of ZIF-8 shell and photocurrent enhancement of polyoxometalate, the polyoxometalate@ZIF-8@ZnO sensors exhibited excellent selectivity for formaldehyde and remarkable sensitivity.

More recently, Zhang et al. (2019d) constructed $Co_3O_4/CoFe_2O_4$ double-shelled nanocages (DSNCs) via a MOF-assisted strategy (Figure 8A). In brief, ZIF-67/PBA core-shell nanocubes were prepared via the ion-exchange method as templates, then the final products obtained by pyrolyzing as-prepared templates at 550 °C in air. Interestingly, $Co_3O_4/CoFe_2O_4$ DSNCs exhibited superior formaldehyde sensing performances included the excellent detection capability of sub-ppm-level formaldehyde, large response (R_g/R_a = 12.7–10 ppm at 139 °C) (Figure 8B), with good high selectivity (Figure 8C) and fast response speed (~4 s). The formaldehyde sensing mechanism of CCFO DSNCs composites is based on the change in the amount of electrons on the surface of the $CoFe_2O_4$ and Co_3O_4 during the ionization of oxygen molecules and the oxidation/reduction reaction of the formaldehyde gas with the $O^{2-}$and O^-. And the enhanced formaldehyde sensing properties of CCFO DSNCs composites can be mainly ascribed to the unique double-shelled nanostructures, large specific surface area, porous structure and p–p heterojunctions ($Co_3O_4/ZnCo_2O_4$).

4.1.4 Xylene sensors

The group of Qu et al. (2016) constructed hollow core-shell $ZnO/ZnCo_2O_4$ nanocages (HCSNCs) via a two-step treatment of ZIF-8 templates, in which ZIF-8/Co–Zn double hydroxides sacrificial templates were first made, and then subsequent thermal treatment of as-made sacrificial templates in air (Figure 9A). The obtained $ZnO/ZnCo_2O_4$ HCSNCs displayed a surface area of 113.2 m^2/g, which is significantly larger than that of ZnO NCs (45.6 m^2/g) and $ZnCo_2O_4$ shells (83.8 m^2/g). Benefits from their unique hollow nanostructure and the formation of $ZnO/ZnCo_2O_4$ heterojunction, the $ZnO/ZnCo_2O_4$ HCSNCs showed good reversibility, high response, and excellent selectivity toward xylene. Another work reported by this group, the $ZnO/Ni_{0.9}Zn_{0.1}O$ double-shelled nanocages (DSNCs) as sensing material, were prepared via the same strategy as above. Similarly, the sensor based on $ZnO/Ni_{0.9}Zn_{0.1}O$ DSNCs showed superior selectivity and high sensitivity to

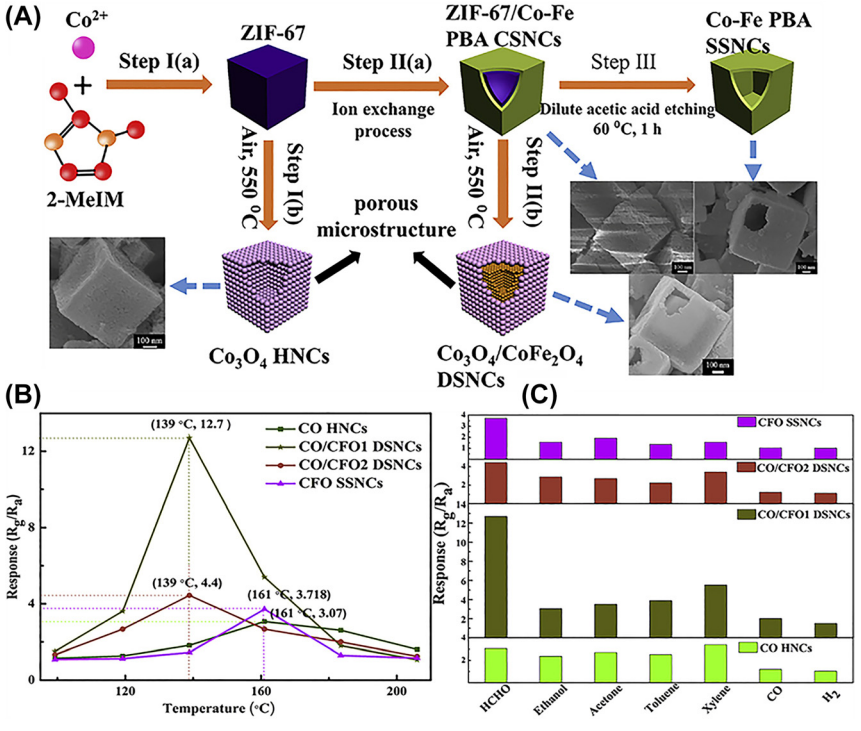

Figure 8: $Co_3O_4/CoFe_2O_4$ double-shell nanocubes for formaldehyde sensing. (A) The fabrication of $Co_3O_4/CoFe_2O_4$ double-shell nanocubes from ZIF-67 nanocubes (Zhang et al. 2019d).
(B) Formaldehyde-sensing properties of $Co_3O_4/CoFe_2O_4$ double-shell nanocubes at different temperature (Zhang et al. 2019d).
(C) The selectivity of $Co_3O_4/CoFe_2O_4$ double-shell nanocubes at room temperature (Zhang et al. 2019d). Copyright permission obtained to reproduce from Elsevier.

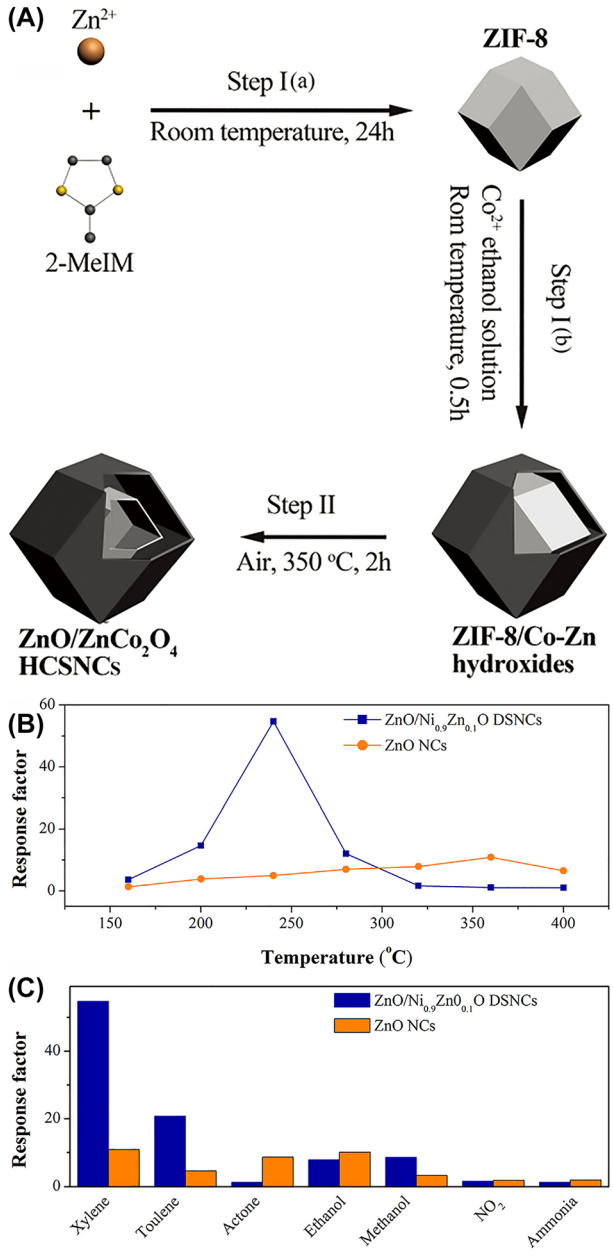

Figure 9: $ZnO/ZnCo_2O_4$ HCSNCs for Xylene-sensing performances. (A) Schematic representation of the synthesis of $ZnO/ZnCo_2O_4$ HCSNCs via a two-step process (Qu et al. 2016). (B, C) Xylene-sensing performances of $ZnO/Ni_{0.9}Zn_{0.1}O$ double-shelled nanocages. Copyright permission obtained to reproduce from Royal Society of Chemistry and Elsevier.

xylene (Figure 9B, C). Moreover, it exhibited obviously enhanced sensing performances compared with ZnO NCs.

Bai et al. (2018) synthesized Co_3O_4/TiO_2 p–n heterojunction through calcination of Ti ion loaded ZIF-67 at 450 °C in air. The Co_3O_4/TiO_2 composites exhibited a response value of 6.17 toward 50 ppm of xylene, which was 5-fold higher compared with singular Co_3O_4 nanoparticles. In addition, this sensor also exhibited fast response/recovery speed, remarkable reversibility, and excellent selectivity due to porous structure and the formation of p–n heterojunction. The xylene sensing mechanism of Co_3O_4/TiO_2 composites heterojunction can be interpreted with the adsorption-reaction mechanism. When Co_3O_4/TiO_2 composites are exposed to air atmosphere, the surface of the Co_3O_4/TiO_2 sensor is susceptible to be occupied by adsorbed oxygen species. Once xylene gas is introduced, O^{2-}(ads) react with xylene molecules, and will form free electrons, CO_2 and H_2O. Eventually, the depletion layer formed in the ethanol gas will be even wider than the depletion layer in air. Jo et al. (2018) reported hollow hierarchical Co_3O_4 nanocages by using rhombic dodecahedral ZIF-67 as precursors showed the highest response toward p-xylene (R_g/R_a = 78.6@5 ppm) at 225 °C among all reported pure Co_3O_4 gas sensing materials. Moreover, the sensor exhibited a high response to toluene (43.8) and remarkable methylbenzene selectivity in the interference of ethanol. Such exceptional sensing performances of the hollow hierarchical Co_3O_4 nanocages were attributed to its unique hierarchical morphology and the excellent catalytic activity of Co_3O_4. Notably, several key parameters such as the morphology, shell thickness, and pore sizes of Co_3O_4 nanocages that significantly determine the gas-sensing properties of the sensor, could be easily controlled via changing the precipitation reaction of the ZIF-67 templates.

4.1.5 n-butanol sensors

Wang et al. (2019) synthesized porous Co_3O_4 assemblies with different morphologies and sizes for sensing n-butanol by direct pyrolysis of Co-MOF (ZIF-67). To investigate the influence of structural features of porous Co_3O_4 assemblies on the gas-sensing performance, four kinds of ZIF-67 precursors were specially designed with different structures. Then, the products acquired by calcining obtained ZIF-67 precursors at 300 °C for 4 h, displayed well-controlled morphologies and sizes. As shown in Figure 3F and Figure 10A–D, the as-synthesized samples Co_3O_4-1, Co_3O_4-3, and Co_3O_4-4 share similar shapes with corresponding precursors ComIM-1, ComIM-3, and ComIM-4, respectively. However, the shape of the Co_3O_4-2 sample was quite different from that of its precursor, ComIM-2. Furthermore, the nanoparticles of Co_3O_4-2 samples exhibited slightly bigger sizes (>10 nm) compared with Co_3O_4-1, Co_3O_4-3, and Co_3O_4-4 with similar sizes (4–7 nm). Meanwhile, the Co_3O_4-1 and Co_3O_4-2 had much lower BET surface areas (17.3 and 11.0 m^2/g, respectively) than Co_3O_4-3 and Co_3O_4-4 (54.2 and 50.9 m^2/g, respectively). Among them, Co_3O_4-4 exhibited the highest

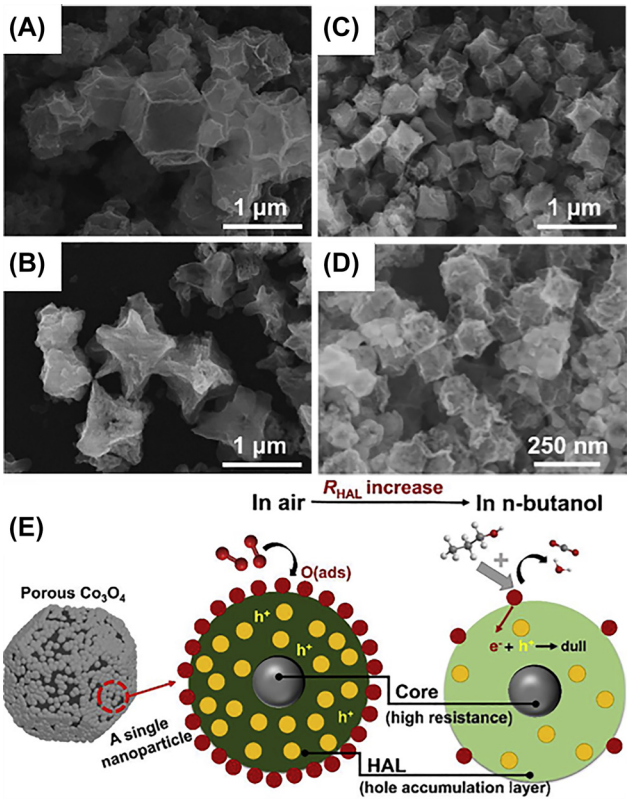

Figure 10: Co_3O_4 nanoparticles and gas sensing. (A–D) SEM images of the obtained Co_3O_4 nanoparticles. (E) The n-butanol sensing mechanism (Wang et al. 2019). Copyright permission obtained to reproduce from Elsevier.

response (R_g/R_a = 21 @100 ppm n-butanol) and the best n-butanol selectivity. In addition, the porous Co_3O_4 sensor showed a relatively low detection limit toward n-butanol (<5 ppm) and high stability. The n-butanol sensing mechanism of Co_3O_4 semiconducting materials is based on surface-resistance controlled mechanism, and the detail n-butanol sensing procedure of porous Co_3O_4 assemblies is depicted in Figure 10E. Clearly, under different atmospheres, various reactions will occur on the surface of the porous Co_3O_4 assembly sensor, including the adsorption of oxygen molecules and the redox reaction of the target gas, while the reaction will be accompanied by changes in both the hole-accumulation layer and the resistance of the surface of the porous Co_3O_4 assembly sensor. This work demonstrated that the structural features of the Co_3O_4 assemblies have a close correlation with their gas-sensing properties. Therefore, this finding can provide a promising strategy to design high-performance gas-sensing materials.

Zhang et al. (2019e) demonstrated that ZnO assemblies exhibited the highest sensing response toward n-butanol. They prepared Zn-MOF (ZIF-8) templates with varied crystallinity and particle size through ligand exchange during the nucleation process. Then, the ZnO assemblies with different pore sizes were obtained by annealing ZIF-8 templates. The as-prepared ZnO-2 with the micropore size of 1 nm showed a high response (37.8@10 ppm) to n-butanol, which was 30 and 20 times gas responses of ammonia and formaldehyde, respectively. In addition, the ZnO-2 sensor exhibited excellent recyclable properties and a relatively low detection limit (<0.1 ppm).

4.1.6 Other VOCs sensors

Koo et al. (2016) reported toluene sensor properties of MOF-derived Pd@ZnO complex catalyst-loaded WO_3 synthesized via electrospinning followed by calcination (Figure 11A). Interestingly, the Pd@ZnO complex catalyst was effectively incorporated into WO_3 nanofibers to produce Pd–ZnO and ZnO–WO_3 heterogeneous structures. Due to the functionalization of the Pd NPs catalyst and the introduction of multi-heterojunction (Figure 11B), the Pd@ZnO-WO_3 sensor showed superior toluene sensitivity (R_a/R_g = 4.37@100 ppb toluene at 350 °C), with rapid gas

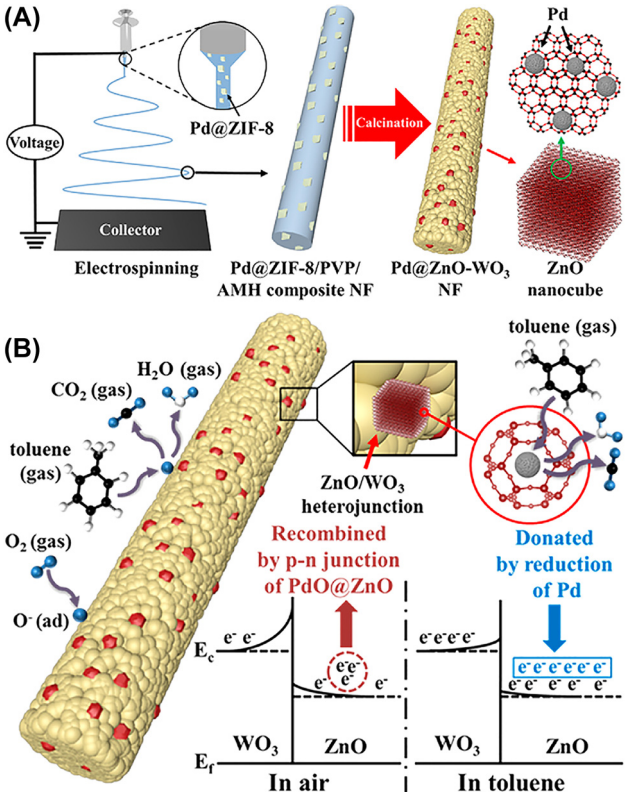

Figure 11: Sensing mechanism of Pd@ZnO-WO_3 nanofibers. (A) The schematic diagram showing the fabrication of Pd@ZnO-WO_3 nanofibers. (B) Schematic diagrams of the sensing mechanism for Pd@ZnO-WO_3 nanofibers (Koo et al. 2016). Copyright permission obtained to reproduce from American Chemical Society.

response time (<20 s). In addition, the sensor exhibited remarkable sensitivity to toluene (R_a/R_g = 22.22@1 ppm) and a negligible response toward the other interfering gases such as ethanol, hydrogen sulfide, nitric monoxide, and ammonia.

Li et al. (2015) synthesized hierarchical ZnO hollow cubes by direct calcination of ZIF-8 templates. The as-synthesized ZnO hollow cubes well maintained the original cube-like morphologies of ZIF-8 and displayed a high BET specific surface area of 45 m^2/g. The as-fabricated chemical sensor based on hierarchical ZnO hollow cubes is able to detect benzene of low concentration (0.1–5.0 ppm) with higher response and the drastically faster response speed compared to the pristine ZnO particles (Figure 12A, B). The enhanced benzene sensing mechanism of ZnO hollow cubes is primarily originated from the unique hierarchical porous nanostructures, and the unique nanostructures of ZnO hollow cubes can provide more exposed oxygen vacancies and faster surface reaction kinetics of benzene molecules, thus realizing the improved sensing performance of hierarchical ZnO hollow cubes. Therefore, this sensor based on hierarchical ZnO hollow cubes has promising application prospects in benzene of low concentrations detection. Ma et al. (2019) have successfully synthesized the porous SnO_2/ZnO flower-like nanostructures by using SnS_2/ZIF-8 as sacrificial template. The as-synthesized SnO_2/ZnO heterogeneous composites displayed a large BET surface area of 108.88 m^2/g, which contributes to enhancing the sensing performances of SnO_2/ZnO heterostructures. Thus, the SnO_2/ZnO showed a high response value of 17.7 toward 50 ppm triethylamine at 200 °C, which increased by about 2.2 times compared to that of pure SnO_2. Moreover, this sensor exhibited rapid response time (~9 s) and excellent selectivity to triethylamine.

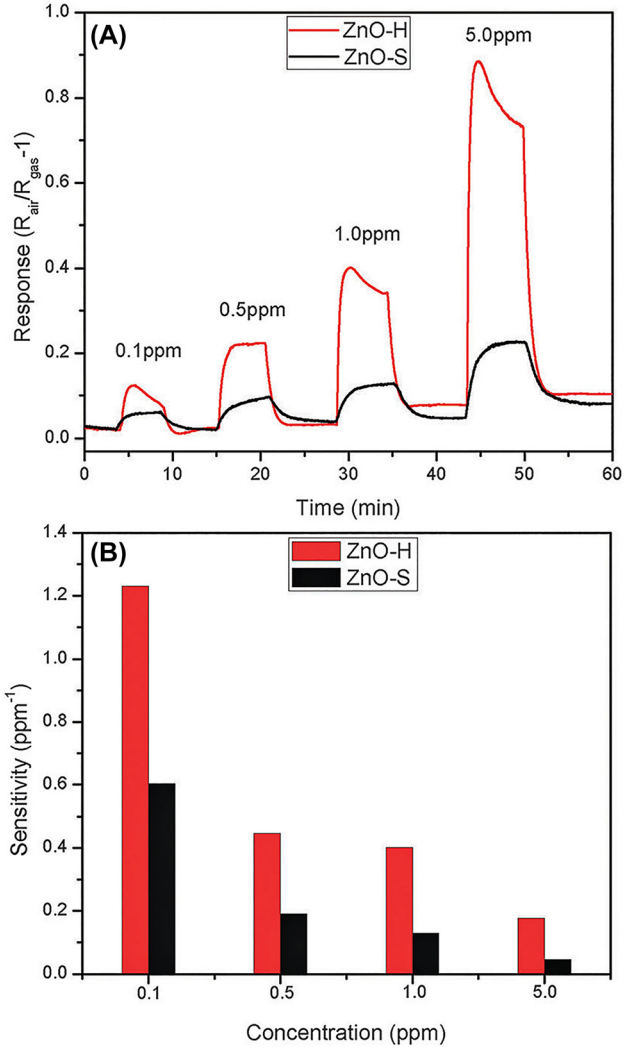

Figure 12: Benzene-sensing properties. (A, B) Benzene-sensing properties (0.1–5 ppm) of ZnO hollow cubes and pristine ZnO particles at 400 °C (Li et al. 2015). Copyright permission obtained to reproduce from Royal Society of Chemistry.

Li et al. (2020b) prepared Co_3O_4/ZnO p–n heterojunctions (Co_3O_4/ZnO NHs) derived from heterogeneous MOFs (ZIF-8@ZIF-67), used for trimethylamine-sensing. The Co_3O_4/ZnO NHs based sensor exhibited superior sensing properties toward trimethylamine included high response (R_{air}/R_g = 232@50 ppm at 190 °C), rapid response time (2.1s@10 ppm), low detection limit (~13 ppb), high trimethylamine selectivity, and excellent stability, compared to pristine ZnO nanocages. In particular, they combined the quasi-*in-situ* XPS studies and DFT calculations to explain the outstanding sensing performances of the sensor. Specifically, through their DFT calculations and Bader charge analysis, it is evident that a significant charge transfer behavior occurred during the sensing of ZnO to trimethylamine gas, which demonstrates that the enhanced sensing mechanism of Co_3O_4/ZnO NHs is attributable to the production of metallic zinc. Meanwhile, the formation of p–n heterojunctions in Co_3O_4/ZnO NHs results in a considerably higher resistance in the air as compared to pure ZnO, which also contributes to the significant enhancement of the trimethylamine gas sensing response. Finally, they attribute the excellent trimethylamine sensing performance to the combined effect of nano-heterojunction formation and the surface metallization.

4.2 Inorganic gas sensors

4.2.1 H_2 sensors

Up to date, MOF(ZIF-8)-based membranes have been extensively studied as an auxiliary filter layer due to its unique properties (e.g., the molecular sieving properties), to improve the poor selectivity of MOSs (e.g., ZnO) gas

sensors. For instance, Wu et al. (2017) developed a hydrogen sensor using core-shell ZnO@ZIF-8 nanorod film as sensing material. As shown in Figure 13A, for pristine ZnO film and the as-synthesized ZnO@ZIF-8 film, the H_2 response increases with increasing working temperature and the highest response value at 250 °C. In contrast with the pristine ZnO film, the as-synthesized ZnO@ZIF-8 film showed a significantly enhanced sensitivity toward H_2. Notably, owing to the strengthened molecular sieving properties of the ZIF-8 thin shell, this ZnO@ZIF-8 film exhibited a negligible CO sensitivity (Figure 13B, C). Similarly, Cui et al. (2018) developed a ZnO@ZIF-8 microrod sensor for the detection of H_2. This sensor exhibited a higher response (8.61@50 ppm), lower optimum working temperature of 125 °C, better selectivity to H_2 over CH_4, C_2H_2, C_2H_4, C_2H_6, and CO compared with pure ZnO microrod sensor. Recently, Khudiar et al. (2020) also synthesized the ZnO@ZIF-8 hybrid materials for selective hydrogen gas detection. The as-fabricated ZnO@ZIF-8 gas sensor displayed an outstanding selective response to H_2 over benzene vapor compared with a raw ZnO sensor. This result is realized by the molecular sieving effect of ZIF-8 coating, hindering the diffusion of larger benzene vapor molecules pass through the pore aperture.

To enhance the selectivity of ZnO nanowires (NWs) sensors, Drobek's group reported ZnO@ZIF-8 nanocomposite NWs for hydrogen detection (Drobek et al. 2016). The obtained nanocomposites exhibited significantly enhanced selectivity to H_2 over C_6H_6 and C_7H_8 as compared to the pure ZnO NWs (Figure 13D–F). In addition, Weber and co-workers reported ZIF-8 nanomembrane coated Pd/ZnO NWs as a highly selective hydrogen detector (Weber et al. 2018). The ZIF-8 coated Pd/ZnO NWs showed a dramatically high response (R_a/R_g = 6.7@50 ppm) to H_2 gas at 200 °C, while negligible responses toward other analytes including C_6H_6, C_7H_8, CH_3COCH_3, and C_2H_5OH. However, the Pd/ZnO NWs showed noticeable responses to all tested gases, which can clearly confirm the poor selectivity of the

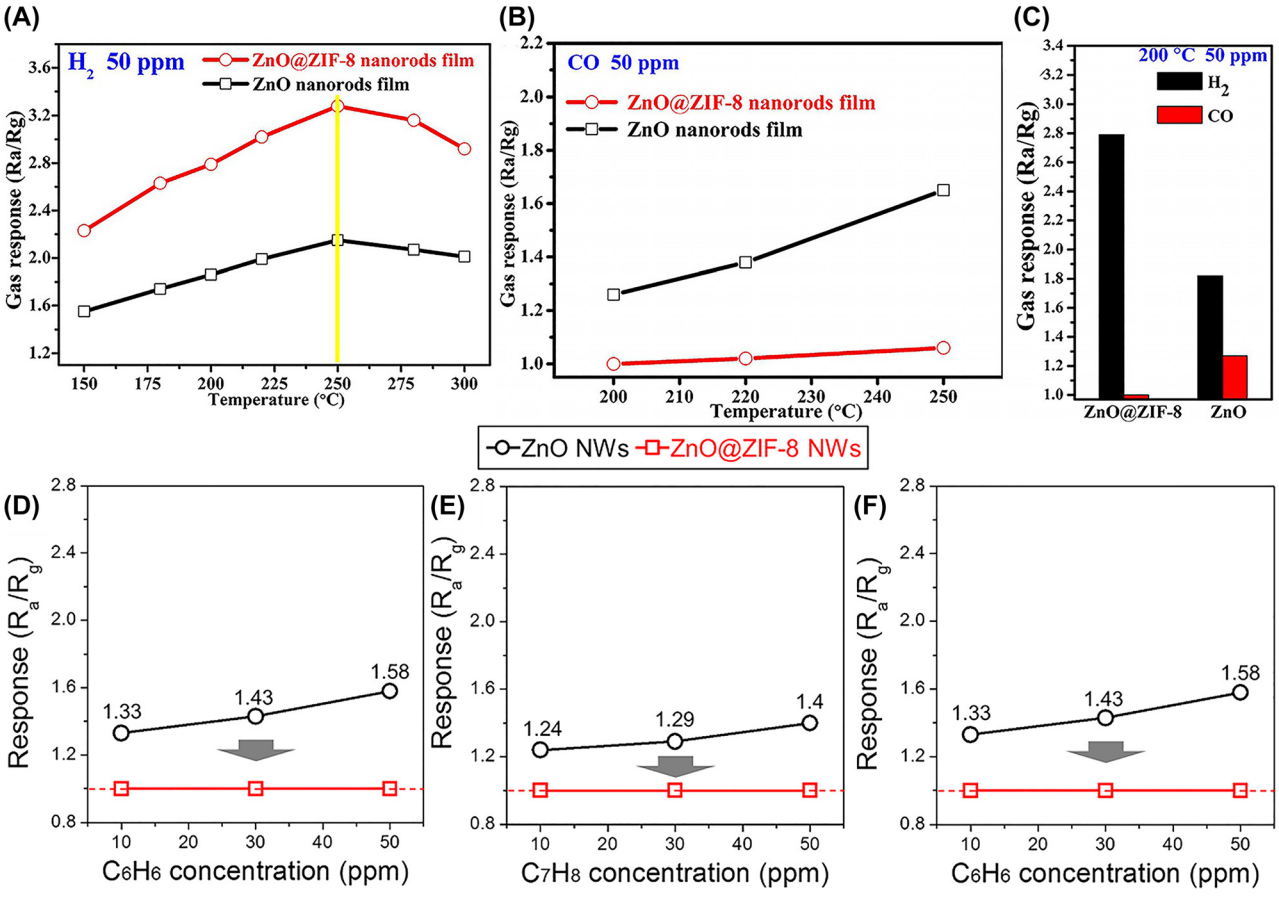

Figure 13: Responses of ZnO@ZIF-8 nanorod. (A) Responses of ZnO@ZIF-8 nanorod and singular ZnO nanorod film toward 50 ppm H_2 at different temperature (150–300 °C) (Wu et al. 2017). (B) Responses of ZnO@ZIF-8 nanorod and singular ZnO nanorod film toward 50 ppm CO (Wu et al. 2017). (C) Selectivity property of ZnO@ZIF-8 film for H_2 over CO at 200 °C (Wu et al. 2017). Response curves of ZnO@ZIF-8 nanowires and ZnO nanowires toward 10, 30, and 50 ppm of (D) H_2, (E) C_7H_8, and (F) C_6H_6 (Drobek et al. 2016). Copyright permission obtained to reproduce from STM Signatory Publisher and American Chemical Society.

gas sensor without ZIF-8 nanomembrane. Such high-performance hydrogen sensors were attributed to the addition of Pd nanoparticles (NPs) and the ZIF-8 nanomembrane overcoat. Furthermore, Jeon et al. (2020) synthesized ZIF-8@ZnO NWs core-shell hybrid nanomaterials and studied the influence of the ZIF-8 membrane on the gas sensing performances of ZnO NWs. In this hybrid system, owing to its unique properties such as excellent gas adsorption capability, exceptional stability, and the molecular sieving effect caused by porous nanostructures, the ZIF-8 membrane can act as dual roles (i.e., the pre-concentrator and the gas separator). Therefore, the ZIF-8@ZnO NWs exhibited a high H_2 response (74.0%@100 ppm of H_2 at 250 °C) with excellent selectivity and retaining a stable response value of 99.1% toward H_2 after 20 days. In general, benefiting from the unique structural characteristics of ZIF-8, it can be combined as a molecular sieve with metal oxides to form metal oxide@ZIF-8 composites, which can significantly improve the sensitivity and selectivity of metal oxide gas sensors, which provides a promising strategy for the development of highly selective sensors, as well as paving the way for other promising ZIF materials.

4.2.2 NO_2 sensors

In 2107, Choi et al. (2017) reported that Pd@ZIF-67 derived PdO-Co_3O_4 HNCs functionalized by single-walled carbon nanotubes (SWCNTs) then integrated on the Ni/Au-colorless polyimide (cPI) heater for detection of NO_2. This sensor exhibited excellent sensing performances toward NO_2, such as high sensitivity ($S = (R_{air}-R_{gas})/R_{air}$ = 44.11% @20 ppm NO_2 at 100 °C), excellent detection capability that could detect as low as 1 ppm NO_2 (S = 3.09%), and high mechanical stability. Similarly, Rui et al. (2018) developed the room-temperature NO_2 sensors based on ZIF-67/multiwalled carbon nanotubes (MWCNTs) and as-derived Co_3O_4/MWCNT hybrid fibers. Those two sensors can detect an ultralow NO_2 gas concentration of 100 ppb with high sensitivity at room temperature. Additionally, they can maintain excellent gas-sensing performance even if they are bent into different angles.

Koo et al. (2018) developed a facile strategy that can effectively confine the few-layered WS_2 nanoplates in hollow carbon nanocages composites derived from ZIF-67 (Figure 14A). Benefiting from the numerous edge sites of

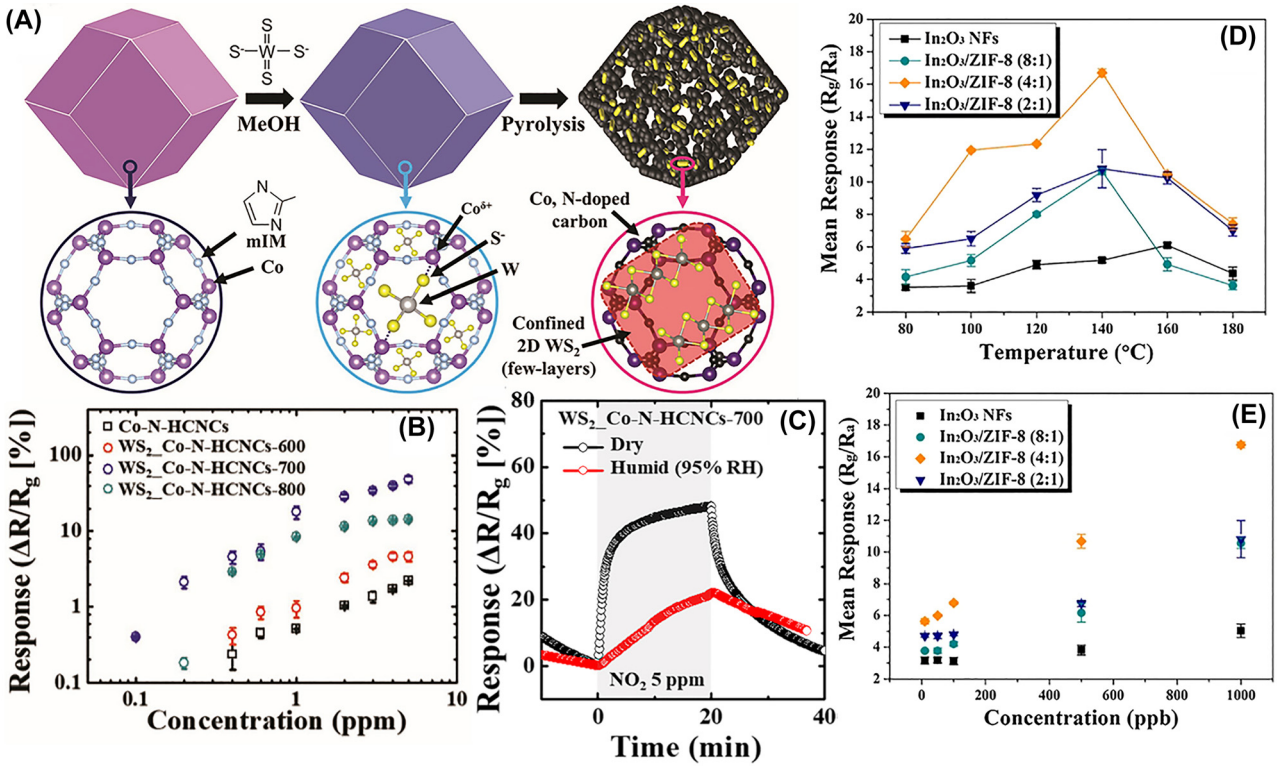

Figure 14: Formation process of WS_2/carbon nanocages composites and Gas sensing. (A) Formation process of WS_2/carbon nanocages composites (Koo et al. 2018). (B) Calculated responses of the various sensors toward NO_2 at room temperature (Koo et al. 2018). (C) Response characteristics of the WS_2/carbon nanocages composites under 95% RH (Koo et al. 2018). (D) Responses to 1 ppm NO_2 versus operating temperature (80–180 °C) (Koo et al. 2018). (E) Response of In_2O_3/ZIF-8 nanofibers toward different concentrations of NO_2 at 140 °C (Liu et al. 2019). Copyright permission obtained to reproduce from STM Signatory Publisher and Elsevier.

WS_2 nanoplates, WS_2/carbon nanocages composites showed dramatically enhanced sensing performances toward NO_2 at room temperature than that of as-derived carbon nanocages composites. The NO_2 sensor based on WS_2/carbon nanocages composites displayed high sensitivity toward NO_2 ($\Delta R/R_g$ = 48.2%@5 ppm) with a low detection limit of 100 ppb at room temperature (Figure 14B), good NO_2 selectivity, excellent NO_2 sensing stability. In addition, the WS_2/carbon nanocages composites showed a comparatively high response value of 21.8% toward 5 ppm NO_2 even in a high humidity (90% RH), as shown in Figure 14C. Liu et al. (2019) first reported that ZIF-8 nanocrystals coated In_2O_3 nanofibers (NFs) were highly sensitive to NO_2 at an optimal testing temperature of 140 °C. As displayed in Figure 14D, E, the In_2O_3/ZIF-8 NFs heterostructures displayed a much higher response compared with pristine In_2O_3 NFs. And more notably, the In_2O_3/ZIF-8 (4:1) NFs heterostructures sensor could detect NO_2 at an extremely low concentration of 10 ppb, showing a relatively high response value (R_g/R_a = 5.6). Furthermore, the In_2O_3/ZIF-8 (4:1) NFs showed a far faster response/recovery speed (80/133 s) and better humidity resistance than that of the pristine In_2O_3 NFs. He et al. (2021) prepared ZnCo-ZIF intercalated GO nanosheets (ZnCo-ZIF/GN) by a facile solvothermal method for NO_2 detection at room temperature. The ZnCo-ZIF/GN composite showed a high sensing response (R_a/R_g = 54.61) under a RH of 30% towards 100 ppm NO_2. In addition, the ZnCo-ZIF/GN based NO_2 sensor displayed excellent gas selectivity, good stability and a remarkably low detection limit of 10 ppb performance acetone gas sensor. These excellent gas sensing results provide a facile strategy to construct poor conductivity of ZIF with highly conductive graphene nanosheet for constructing advanced high-performance gas-sensing application.

4.2.3 H_2S sensors

Wu et al. (2019b) developed an advanced H_2S sensor based on MOF(ZIF-8)-loaded ZnO nanorods prepared via a self-template method. The sensor showed excellent room-temperature H_2S-sensing performance. In particular, the as-made sensor not only has the unique structural features of porous ZIF-8 but also possess attractive gas sensing performances of semiconductor-metal-oxide. Thus, the sensor exhibited excellent sensing performances toward target gas H_2S. The ZIF-8/ZnO showed a significantly enhanced sensing response to H_2S ($(\Delta R)/R_a$ = 52.1@10 ppm) at room temperature, which increased by 15 times compared with pure ZnO nanorods (Figure 15A). It is noteworthy that the response values of ZIF-8/ZnO nanorods to H_2S gas only slightly decreased even when the humidity increased to 70%, as shown in Figure 15B. In addition, the sensor exhibited remarkable H_2S selectivity, ppb-level detection limit (~50 ppb), and superior stability (i.e., excellent hydrophobic property). Zhou et al. (2020)

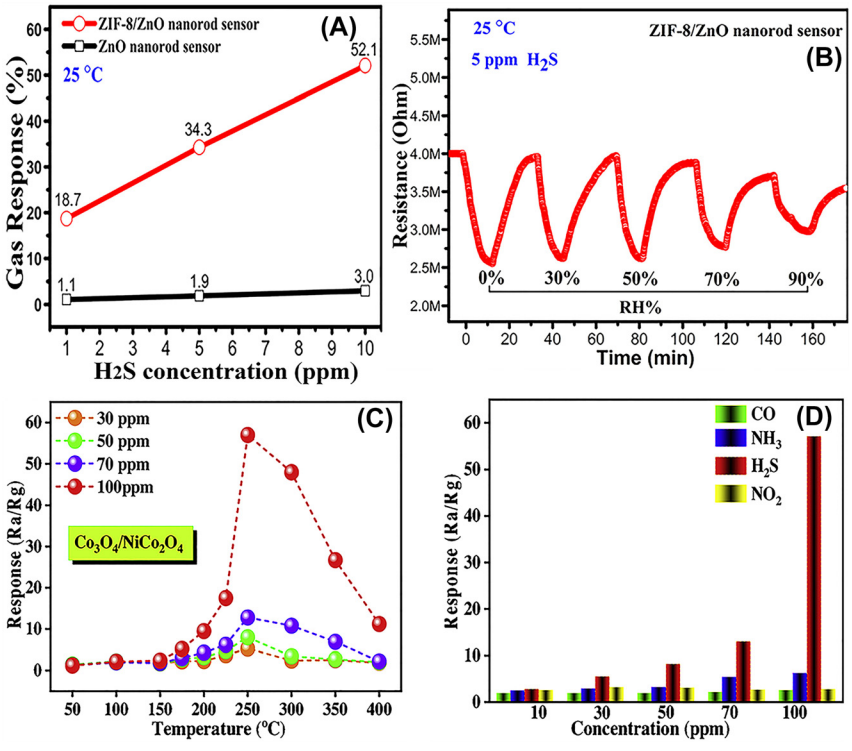

Figure 15: Responses to H_2S gas. (A) The response of raw ZnO and ZIF-8-loaded ZnO nanorod toward H_2S at room temperature. (B) Response properties of ZIF-8-loaded ZnO nanorod under different humidity from 0 to 90% (Wu et al. 2019). (C) The response of $Co_3O_4/NiCo_2O_4$ DSNCs from ZIF-67 rhombododecahedron at different temperatures (Tan et al. 2020). (D) Selectivity properties of $Co_3O_4/NiCo_2O_4$ DSNCs toward various analytes at 50 ppm (Tan et al. 2020). Copyright permission obtained to reproduce from Elsevier.

prepared 3D inverse opal (3DIO) Pt/ZnO nanocomposites via the thermolysis of 3DIO Pt NPs@ZIF-8 template for the sensing of trace-level H_2S gas. The obtained 3DIO Pt/ZnO nanocomposites featured an exceptionally high surface area of 171.6 m^2/g. Further, taking advantage of the size effect of noble metal Pt NPs, 3DIO Pt/ZnO nanocomposites exhibited a high response (11.2) toward 1 ppm of H_2S at working temperature of 320 °C, an ultralow detection limit (~25 ppb), excellent H_2S sensitivity, and long-term stability.

Using ZIF-67/Ni-Co yolk-shell nanostructure as the templates, our group reported the template-assisted synthesis of $Co_3O_4/NiCo_2O_4$ DSNCs as gas sensing materials for detection of H_2S (Tan et al. 2020). The as-synthesized $Co_3O_4/NiCo_2O_4$ DSNCs displayed a large BET surface area of 103 m^2/g. As shown in Figure 15C, for the synthesized $Co_3O_4/NiCo_2O_4$ DSNCs H_2S gas sensors, the response values at different gas concentrations (30, 50, 70 and 100 ppm) all exhibit an increase first with increasing operating temperature from 50 to 250 °C, and then a decrease in response at higher operating temperatures. The $Co_3O_4/NiCo_2O_4$ DSNCs exhibited the best sensitivity and selectivity to H_2S, with negligible responses to other analytes. In particular, this sensor showed superior response and selectivity toward 100 ppm of H_2S at 250 °C (Figure 15D). Such excellent sensing performances demonstrated that hollow double-shelled architectures have the remarkable potential in the fabrication of superior gas sensors.

4.2.4 CO/CO_2 sensors

Matatagui et al. (2018) constructed a chemoresistive sensor based on ZIF-8/ZIF-67 nanostructures for the detection of CO, H_2, NO_2, toluene and ethanol. This chemoresistive sensor could detect these target gases with significant resistance change at relatively low concentrations (down to 10 ppm). Notably, the ZIF-8/ZIF-67 combination-based sensor exhibited significantly enhanced responses to toluene and hydrogen of 10 ppm compared with ZIF-67 nanocrystals. In addition, it showed rapid response, excellent repeatability, and reversibility. Qin et al. (2020) prepared Co_3O_4 nanostructures with numerous octahedral active Co^{3+} sites, derived from ZIF-67 precursors by controlling the calcination conditions (i.e., calcination temperature and heating rate). Owing to the high activity of Co^{3+} for CO oxidation, the as-prepared Co_3O_4 nanostructures with abundant active Co^{3+} sites showed significantly improved CO gas sensing properties, compared to Co_3O_4 nanoparticles. For example, the sample obtained through calcination of ZIF-67 precursor at 300 with heating rate of 1 °C min^{-1} exhibited an ultrahigh response (~20 times) toward 100 ppm of CO at a significantly lower working temperature compared with Co_3O_4 nanoparticles. Moreover, this sensor showed fast response/recovery speed (10/2 s), low detection limit (at least 500 ppb), and excellent CO selectivity and superior stability. To further enhance the interaction between CO_2 gas and SnO_2 surface, Me et al. (2018) synthesized core-shell SnO_2 @ZIF-67 hybrid nanostructure to utilize excellent CO_2 capturing properties of ZIF-67 and the synergistic effects of the hybrid nanostructure. The response of SnO_2 @ZIF-67 hybrid nanostructure was 12-fold in enhancement for 50% CO_2 sensing than the pristine SnO_2 sensor. This sensor exhibited the highest gas response (16.5 ± 2.1% toward 0.5% CO_2) at 205 °C, among the reported SnO_2-based sensors. In addition, the as-prepared hybrid nanostructure showed remarkable recovery time (22.04 ± 4.33 s for 50% CO_2, 25.5 ± 4.5 s for 5000 ppm CO_2) and a relatively low operating temperature of 205 °C. These gas sensing results show that the assembly of ZIF-X (8, 67) on metal oxide nanoparticles is an attractive prospect for achieving high performance gas sensing properties.

4.2.5 Other inorganic gas sensors

Reddy et al. (2020) synthesized pure MOF (ZIF-8) via a facile chemical route method as gas-sensing material for detection of NH_3 at room temperature. However, the NH_3 sensing performances of as-prepared ZIF-8 were unsatisfactory. For instance, the ZIF-8 sensor showed a relatively low response value (9) toward 100 ppm concentration of NH_3.

Furthermore, the semiconductor gas sensing material (ZnO nanowires) hybridized with ZIF-8 nanocrystals prepared by Jeon et al. (2020) also displayed sensitivity to NO_2 and NH_3. Take advantage of this unique hybrid nanostructure, ZIF-8@ZnO nanowires showed excellent responses (62.3% for 20 ppm NO_2, and 77.2% for 10 ppm NH_3) at 250 °C, excellent long-term stability and low gas detection limit (1 ppm for NO_2, and 500 ppb for NH_3). Additionally, the ZIF-8@ZnO hybrid nanostructure sensor exhibited significantly enhanced selectivity at 250 °C for NO_2 and NH_3 over CH_4 and C_3H_8 compared with the sensor based on pure ZnO nanowires (Figure 16A, B).

Li et al. (2018a) prepared a CoZn-NCNTs material through the direct pyrolysis of zinc doped ZIF-67 (i.e., bimetallic MOFs ZnZIF-67) under Ar atmosphere. The synthesized CoZn-NCNTs retain the nano-polyhedral morphology of the ZnZIF-67 with a high surface area of 446.35 m^2/g, and have abundant interconnected CNTs on the external faces (Figure 16C). As shown in Figure 16D, the CoZn-NCNTs exhibited remarkable performances for the

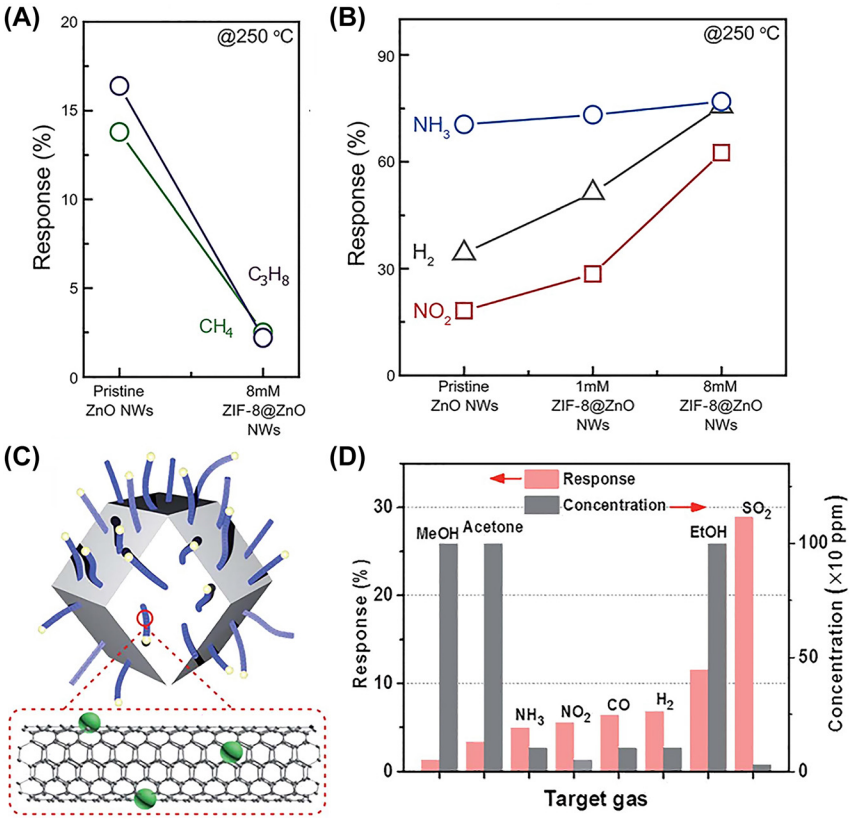

Figure 16: The selectivity (A) and response (B) of pure ZnO nanowires and ZIF-8@ZnO hybrid nanostructure to various target gases (Jeon et al. 2020). (C) Schematic illustration of the nanostructure of CoZn-NCNTs. (D) SO_2-sensing properties of the CoZn-NCNTs sensor toward various toxic gases (Li et al. 2018). Copyright permission obtained to reproduce from Elsevier and Royal Society of Chemistry.

sulfur dioxide (SO_2) detection at room temperature. For instance, it showed a high response value ($(\Delta R/R_0) = 28.9\%$) toward 30 ppm of SO_2 with fast response/recovery speed (78/32 s). In addition, the CoZn-NCNTs exhibited excellent SO_2 selectivity, superior chemical stability and response repeatability. To deeply understand the SO_2 sensing mechanism of CoZn-NCNTs, they explored the effect of the doped Zn on the band structure of nanotube using first-principles calculations, and the calculations showed that the doped Zn would alter the band structure of the CNTs, which led to a significant enhancement of the SO_2 adsorption capacity, ultimately enabling the CoZn-NCNTs to exhibit excellent SO_2 sensing performance. This work presents a novel zeolitic imidazolate frameworks based strategy for the preparation of the excellent sensing materials for the detection of SO_2 gas at room temperature.

5 Summary and perspective

In summary, we have discussed the recent development of ZIF-X (8, 67) based nanostructures for gas-sensing applications, including pristine ZIF-X (8, 67), ZIF-X (8, 67) based membranes, and derivatives. To obtain high-performance ZIF-X (8, 67) based gas sensors, several promising strategies have been explored in recent years. Through the rational heteroatom-doping, nanostructure design, and construction of heterojunction, ZIF-X (8, 67) based sensing materials could provide superior gas-sensing performances. In particular, we summarized which nanostructures are best to choose for detecting a specific target gas based on the crucial parameters of gas-sensing applications including sensitivity, cross-selectivity, response time, and long-term stability (Table 4). As an excellent subfamily of the crystalline materials MOFs, ZIFs have ultrahigh surface areas, diverse structures, high hydrothermal robustness, and excellent chemical resistance. Featuring these desirable properties, ZIFs have gained extensive interest in widespread fields, including electrochemistry, gas storage and separation, and sensing. In particular, ZIF-8 and ZIF-67 are ZIF materials of the most representative, which exhibit superior thermal and chemical stabilities, and unique structural properties.

In this review, we summarized the current advances of ZIF-X (8, 67) based nanostructures, especially for gas-sensing applications. Firstly, due to their porous structure with tunable pore aperture and exceptional stabilities, ZIF-X (8, 67) materials are especially suitable for gas storage including CO_2, H_2, and CH_4, and ZIF-X (8, 67) based mixed matrix membranes have also shown promising

Table 4: The summary of the optimal ZIF-X (8, 67) based nanostructures for the detection of a specific target gas up to now.

ZIF	Metal oxide	Response	Target gas	References
ZIF-8	ZnO@MoS_2	150 at 0.5 ppm	Acetone	Chang et al. (2020)
ZIF-67	Co_3O_4	222 at 100 ppm	Ethanol	Zhang et al. (2020b)
ZIF-67/Co–Fe	Co_3O_4/$CoFe_2O_4$	12.7 at 10 ppm	Formaldehyde	Zhang et al. (2019b)
ZIF-67	Co_3O_4	78.6 at 5 ppm	Xylene	Jo et al. (2018)
Pd@ ZIF-8/PVP/AMH	Pd@ZnO–WO_3	22.2 at 1 ppm	Toluene	Koo et al. (2016)
ZIF-8	ZnO	37.8 at 10 ppm	n-Butanol	Zhang et al. (2019c)
SnS_2/ZIF-8	SnO_2/ZnO	17.7 at 50 ppm	Triethylamine	Ma et al. (2019)
ZIF-8@ZIF-67	Co_3O_4/ZnO	232 at 50 ppm	Trimethylamine	Li et al. (2020b)
ZIF-8	ZnO	1.21 at 0.1 ppm	Benzene	Li et al. (2015)
ZnO@ZIF-8	/	72.3 at 100 ppm	H_2	Jeon et al. (2020)
WS_4_ZIF-67	WS_2_Co–N–HCNC	48.2 at 5 ppm	NO_2	Koo et al. (2018)
Pt@ZIF-8	Pt/ZnO	11.2 at 1 ppm	H_2S	Zhou et al. (2020b)
ZIF-67	Co_3O_4	220 at 100 ppm	CO	Qin et al. (2020)
SnO_2@ZIF-67	/	16.5 at 5000 ppm	CO_2	Me et al. (2018)
ZnO@ZIF-8	/	77.7 at 10 ppm	NH_3	Jeon et al. (2020)
Zinc doped ZIF-67	CoZn-NCNTs	28.9 at 30 ppm	SO_2	Li et al. (2018a)

potential in the excellent gas separation applications such as CO_2/CH_4, H_2/CH_4, C_3H_6/C_3H_8 and so on. Furthermore, more novel strategies are needed to develop ZIF-X (8, 67) based materials to further expand those gas storage and gas separation applications in the future.

Lastly, we specifically emphasize the nanostructure-sensing properties relationship in gas-sensing applications. In particular, we focused on the key parameters of the gas sensors (sensitivity, response rate, selectivity, stability, and sensing mechanisms) and detailed the sensing performances of ZIF-X (8, 67) based nanostructures toward inorganic analytes and VOCs. To obtain a high-performance gas sensor (i.e., high sensitivity and selectivity, fast response, low cost, and remarkable long-term stability), numerous strategies have been suggested for developing the unique ZIF-X (8, 67) based nanostructures (pure ZIF, ZIF-X (8, 67) based nanocomposite and derivatives), and the obtained nanostructures possess numerous extraordinary advantages. Firstly, these unique nanostructures possess huge surface area and a great deal of active sites, which can significantly promote the target gases adsorptions or surface reactions and can dramatically enhance the sensitivity of gas sensors. Secondly, the easily adjustable pore sizes permit them to serve as molecular sieves, which can dramatically enhance the selectivity of gas sensors. In addition, the sensing materials derived from ZIF-X (8, 67) based nanostructures would exhibit high porosity during pyrolysis, which is crucial for sensing performance due to their excellent gas accessibility, ultra-high surface area, and innumerable exposure active sites. It is noteworthy that mesoporous structures are the most common amongst sensing materials with porous nanostructure and are most beneficial for enhancing the sensing properties. Lastly, the ZIF-X (8, 67) based nanostructures possess superior thermal and chemical stability and can be stable in some harsh environments. Therefore, ZIF-X (8, 67)-based nanostructures exhibit excellent stability including good repeatability and long-term stability during gas-sensitive reactions while being utilized as sensitive materials. Therefore, these novel ZIF-X (8, 67) based nanostructures have great potential to be efficient sensing materials for wide applications in environmental protection (e.g., environmental harmful gas sensors), medical diagnosis (e.g., exhaled breath analyzers), indoor air quality monitoring, and food technology.

Despite some innovative advancements achieved in ZIF-X (8, 67) based nanostructures for gas sensors, several worthwhile directions are still pursued. (1) Metal oxides derived from ZIF-X (8, 67) nanostructures, tend to require high operating temperatures in gas sensing reactions, for which graphene or conductive polymers can be combined with ZIF-X (8, 67) based nanostructures to achieve lower operating temperatures as well as room temperature operation. (2) Low detection limits and high response are also important in practical applications, which may be further enhanced by the construction of novel heterostructures and the introduction of nanoscale metal NPs catalysts (e.g. Pd, Pt, Au, Ag, etc.) to obtain higher response values and lower detection limits. (3) Excellent selectivity is a key factor in achieving accuracy in gas sensors, and this can be achieved by developing simple and promising methods to design homogeneous ZIF membranes with

specific pore sizes to improve their ability to act as molecular sieves against interfering gases, thus enabling highly selective sensors. All in all, further development of ZIF-X (8, 67) based nanostructure (pure ZIF, ZIF membrane, and their derivatives) is still needed and can further expand their possible applications in the future.

Author contributions: All the authors have accepted responsibility for the entire content of this submitted manuscript and approved submission.

Research funding: This work was supported by the National Natural Science Foundation of China (52172069, 51950410596), the Key Research and Development Plan (BE2019094), the Six Talent Peaks Project (TD-XCL-004) and the Qing Lan Project ([2016]15) of Jiangsu Province.

Conflict of interest statement: The authors declare no conflicts of interest regarding this article.

References

Aceituno Melgar, V.M., Kim, J., and Othman, M.R. (2015). Zeolitic imidazolate framework membranes for gas separation: a review of synthesis methods and gas separation performance. J. Ind. Eng. Chem. 28: 1–15.

Adatoz, E., Avci, A., and Keskin, S. (2015). Opportunities and challenges of MOF-based membranes in gas separations. Separ. Purif. Technol. 152: 207–239.

Akbari Beni, F. and Niknam Shahrak, M. (2020). Alkali metals-promoted capacity of ZIF-8 and ZIF-90 for carbon capturing: a molecular simulation study. Polyhedron 178: 114338.

Anh Phan, C.J.D., Fernando, J., Uribe-Romo, Carolyn, B., Knobler, O'keeffe, M., and Yaghi, O.M. (2009). Synthesis, structure, and carbon dioxide capture properties of zeolitic imidazolate frameworks. Acc. Chem. Res. 43: 58–67.

Bai, S., Tian, K., Tian, Y., Guo, J., Feng, Y., Luo, R., Li, D., Chen, A., and Liu, C.C. (2018). Synthesis of Co_3O_4/TiO_2 composite by pyrolyzing ZIF-67 for detection of xylene. Appl. Surf. Sci. 435: 384–392.

Bhargav, K.K., Maity, A., Ram, S., and Majumder, S.B. (2014). Low temperature butane sensing using catalytic nano-crystalline lanthanum ferrite sensing element. Sens. Actuators, B 195: 303–312.

Blanco-Rodriguez, A., Camara, V.F., Campo, F., Becheran, L., Duran, A., Vieira, V.D., De Melo, H., and Garcia-Ramirez, A.R. (2018). Development of an electronic nose to characterize odours emitted from different stages in a wastewater treatment plant. Water Res. 134: 92–100.

Brekalo, I., Yuan, W., Mottillo, C., Lu, Y., Zhang, Y., Casaban, J., Holman, K.T., James, S.L., Duarte, F., Williams, P.A., et al. (2020). Manometric real-time studies of the mechanochemical synthesis of zeolitic imidazolate frameworks. Chem. Sci. 11: 2141–2147.

Chang, X., Li, X., Qiao, X., Li, K., Xiong, Y., Li, X., Guo, T., Zhu, L., and Xue, Q. (2020). Metal-organic frameworks derived $ZnO@MoS_2$ nanosheets core/shell heterojunctions for ppb-level acetone detection: ultra-fast response and recovery. Sens. Actuators, B 304: 127430.

Chen, E.X., Yang, H., and Zhang, J. (2014). Zeolitic imidazolate framework as formaldehyde gas sensor. Inorg. Chem. 53: 5411–5413.

Chen, Y., Li, H., Ma, Q., Che, Q., Wang, J., Wang, G., and Yang, P. (2018). ZIF-8 derived hexagonal-like α-$Fe_2O_3/ZnO/Au$ nanoplates with tunable surface heterostructures for superior ethanol gas-sensing performance. Appl. Surf. Sci. 439: 649–659.

Chen, Y., Wu, H., Yuan, Y., Lv, D., Qiao, Z., An, D., Wu, X., Liang, H., Li, Z., and Xia, Q. (2020). Highly rapid mechanochemical synthesis of a pillar-layer metal-organic framework for efficient CH_4/N_2 separation. Chem. Eng. J. 385: 123836.

Cheng, P. and Hu, Y.H. (2014). H_2O-functionalized zeolitic Zn(2-methylimidazole)$_2$ framework (ZIF-8) for H_2 storage. J. Phys. Chem. C 118: 21866–21872.

Choi, S.J., Choi, H.J., Koo, W.T., Huh, D., Lee, H., and Kim, I.D. (2017). Metal-organic framework-templated PdO-Co_3O_4 nanocubes functionalized by SWCNTs: improved NO_2 reaction kinetics on flexible heating film. ACS Appl. Mater. Interfaces 9: 40593–40603.

Cui, F., Chen, W., Jin, L., Zhang, H., Jiang, Z., and Song, Z. (2018). Fabrication of ZIF-8 encapsulated ZnO microrods with enhanced sensing properties for H_2 detection. J. Mater. Sci. Mater. Electron. 29: 19697–19709.

Cui, W., Kang, X., Zhang, X., Zheng, Z., and Cui, X. (2019). Facile synthesis of porous cubic microstructure of Co_3O_4 from ZIF-67 pyrolysis and its Au doped structure for enhanced acetone gas-sensing. Physica E 113: 165–171.

Ding, D., Xue, Q., Lu, W., Xiong, Y., Zhang, J., Pan, X., and Tao, B. (2018). Chemically functionalized 3D reticular graphene oxide frameworks decorated with MOF-derived Co_3O_4: towards highly sensitive and selective detection to acetone. Sens. Actuators, B 259: 289–298.

Dong, C., Li, A., Wang, C., Li, J., Gao, H., Chen, X., Wang, Y., Li, L., Zheng, Y., and Wang, G. (2022). Engineering attractive interaction in ZIF-based phase change materials for boosting electro- and photo- driven thermal energy storage. Chem. Eng. J. 430: 133007.

Drobek, M., Kim, J.H., Bechelany, M., Vallicari, C., Julbe, A., and Kim, S.S. (2016). MOF-based membrane encapsulated ZnO nanowires for enhanced gas sensor selectivity. ACS Appl. Mater. Interfaces 8: 8323–8328.

Faustini, M., Kim, J., Jeong, G.Y., Kim, J.Y., Moon, H.R., Ahn, W.S., and Kim, D.P. (2013). Microfluidic approach toward continuous and ultrafast synthesis of metal-organic framework crystals and hetero structures in confined microdroplets. J. Am. Chem. Soc. 135: 14619–14626.

Furukawa, H., Cordova, K.E., keeffe, M., and Yaghi, O.M. (2013). The chemistry and applications of metal-organic frameworks. Science 341: 1230444.

Gong, X., Wang, Y., and Kuang, T. (2017). ZIF-8-based membranes for carbon dioxide capture and separation. ACS Sustain. Chem. Eng. 5: 11204–11214.

Guan, W., Dai, Y., Dong, C., Yang, X., and Xi, Y. (2020). Zeolite imidazolate framework (ZIF)-based mixed matrix membranes for CO_2 separation: a review. J. Appl. Polym. Sci. 137: 48968.

Guo, H., Shi, F., Ma, Z., and Liu, X. (2010). Molecular simulation for adsorption and separation of CH_4, H_2 in zeolitic imidazolate frameworks. J. Phys. Chem. C 114: 12158–12165.

Guo, R., Wang, H., Tian, R., Shi, D., Li, H., Li, Y., and Liu, H. (2020). The enhanced ethanol sensing properties of CNT@$ZnSnO_3$ hollow boxes derived from Zn-MOF(ZIF-8). Ceram. Int. 46: 7065–7073.

Han, X., Tao, K., Wang, D., and Han, L. (2018). Design of a porous cobalt sulfide nanosheet array on Ni foam from zeolitic imidazolate frameworks as an advanced electrode for supercapacitors. Nanoscale 10: 2735–2741.

He, L., Zhang, W., Wu, H., and Zhao, Y. (2021). Zn–Co zeolitic imidazolate framework nanoparticles intercalated in graphene nanosheets for room-temperature NO_2 sensing. ACS Appl. Nano Mater. 4: 3998–4006.

Houndonougbo, Y., Signer, C., He, N., Morris, W., Furukawa, H., Ray, K.G., Olmsted, D.L., Asta, M., Laird, B.B., and Yaghi, O.M. (2013). A combined experimental–computational investigation of methane adsorption and selectivity in a series of isoreticular zeolitic imidazolate frameworks. J. Phys. Chem. C 117: 10326–10335.

Hu, C., Bai, Y., Hou, M., Wang, Y., Wang, L., Cao, X., Chan, C.W., Sun, H., Li, W., Ge, J., et al. (2020). Defect-induced activity enhancement of enzyme-encapsulated metal-organic frameworks revealed in microfluidic gradient mixing synthesis. Sci. Adv. 6: 5785.

Jang, J.S., Koo, W.T., Choi, S.J., and Kim, I.D. (2017). Metal organic framework-templated chemiresistor: sensing type transition from P-to-N using hollow metal oxide polyhedron via galvanic replacement. J. Am. Chem. Soc. 139: 11868–11876.

Jeon, I.S., Bae, G., Jang, M., Song, W., Myung, S., Lee, S.S., Jung, H.K., Hwang, J., and An, K.S. (2020). A synergistic combination of zinc oxide nanowires array with dual-functional zeolitic imidazolate framework-8 for hybrid nanomaterials-based gas sensors. Composites, Part B 180: 107552.

Jo, Y.M., Kim, T.H., Lee, C.S., Lim, K., Na, C.W., Abdel-Hady, F., Wazzan, A.A., and Lee, J.H. (2018). Metal-organic framework-derived hollow hierarchical Co_3O_4 nanocages with tunable size and morphology: ultrasensitive and highly selective detection of methylbenzenes. ACS Appl. Mater. Interfaces 10: 8860–8868.

Kaneti, Y.V., Dutta, S., Hossain, M.S.A., Shiddiky, M.J.A., Tung, K.L., Shieh, F.K., Tsung, C.K., Wu, K.C.W., and Yamauchi, Y. (2017). Strategies for improving the functionality of zeolitic imidazolate frameworks: tailoring nanoarchitectures for functional applications. Adv. Mater. 29: 1700213.

Khudiar, A.I., Elttayef, A.K., Khalaf, M.K., and Oufi, A.M. (2020). Fabrication of ZnO@ZIF-8 gas sensors for selective gas detection. Mater. Res. Express 6: 126450.

Kong, G.Q., Ou, S., Zou, C., and Wu, C.D. (2012). Assembly and post-modification of a metal-organic nanotube for highly efficient catalysis. J. Am. Chem. Soc. 134: 19851–19857.

Koo, W.T., Cha, J.H., Jung, J.W., Choi, S.J., Jang, J.S., Kim, D.H., and Kim, I.D. (2018). Few-layered WS_2 nanoplates confined in Co, N-doped hollow carbon nanocages: abundant WS_2 edges for highly sensitive gas sensors. Adv. Funct. Mater. 28: 1802575.

Koo, W.T., Choi, S.J., Kim, S.J., Jang, J.S., Tuller, H.L., and Kim, I.D. (2016). Heterogeneous sensitization of metal-organic framework driven metal@metal oxide complex catalysts on an oxide nanofiber scaffold toward superior gas sensors. J. Am. Chem. Soc. 138: 13431–13437.

Koo, W.T., Jang, J.S., Choi, S.J., Cho, H.J., and Kim, I.D. (2017a). Metal-organic framework templated catalysts: dual sensitization of PdO–ZnO composite on hollow SnO_2 nanotubes for selective acetone sensors. ACS Appl. Mater. Interfaces 9: 18069–18077.

Koo, W.T., Jang, J.S., and Kim, I.D. (2019). Metal-organic frameworks for chemiresistive sensors. Chem 5: 1938–1963.

Koo, W.T., Yu, S., Choi, S.J., Jang, J.S., Cheong, J.Y., and Kim, I.D. (2017b). Nanoscale PdO catalyst functionalized Co_3O_4 hollow nanocages using MOF templates for selective detection of acetone molecules in exhaled breath. ACS Appl. Mater. Interfaces 9: 8201–8210.

Kreno, L.E., Leong, K., Farha, O.K., Allendorf, M., Van Duyne, R.P., and Hupp, J.T. (2011). Metal–organic framework materials as chemical sensors. Chem. Rev. 112: 1105–1125.

Kukkar, P., Kim, K.H., Kukkar, D., and Singh, P. (2021). Recent advances in the synthesis techniques for zeolitic imidazolate frameworks and their sensing applications. Coord. Chem. Rev. 446: 214109.

Li, B., Wen, H.M., Zhou, W., and Chen, B. (2014a). Porous metal-organic frameworks for gas storage and separation: what, how, and why? J. Phys. Chem. Lett. 5: 3468–3479.

Li, H., Li, L., Lin, R.-B., Zhou, W., Zhang, Z., Xiang, S., and Chen, B. (2019). Porous metal-organic frameworks for gas storage and separation: status and challenges. EnergyChem 1: 100006.

Li, J.R., Sculley, J., and Zhou, H.C. (2012). Metal-organic frameworks for separations. Chem. Rev. 112: 869–932.

Li, M., Liu, Y., Li, F., Shen, C., Kaneti, Y.V., Yamauchi, Y., Yuliarto, B., Chen, B., and Wang, C.C. (2021). Defect-rich hierarchical porous UiO-66(Zr) for tunable phosphate removal. Environ. Sci. Technol. 55: 13209–13218.

Li, Q., Wu, J., Huang, L., Gao, J., Zhou, H., Shi, Y., Pan, Q., Zhang, G., Du, Y., and Liang, W. (2018a). Sulfur dioxide gas-sensitive materials based on zeolitic imidazolate framework-derived carbon nanotubes. J. Mater. Chem. A. 6: 12115–12124.

Li, R., Ren, X., Zhao, J., Feng, X., Jiang, X., Fan, X., Lin, Z., Li, X., Hu, C., and Wang, B. (2014b). Polyoxometallates trapped in a zeolitic imidazolate framework leading to high uptake and selectivity of bioactive molecules. J. Mater. Chem. A. 2: 2168–2173.

Li, W., Wu, X., Liu, H., Chen, J., Tang, W., and Chen, Y. (2015). Hierarchical hollow ZnO cubes constructed using self-sacrificial ZIF-8 frameworks and their enhanced benzene gas-sensing properties. New J. Chem. 39: 7060–7065.

Li, X., Cai, Z., Jiang, L.P., He, Z., and Zhu, J.J. (2020a). Metal-ligand coordination nanomaterials for biomedical imaging. Bioconjugate Chem. 31: 332–339.

Li, X., Zheng, S., Jin, L., Li, Y., Geng, P., Xue, H., Pang, H., and Xu, Q. (2018b). Metal-organic framework-derived carbons for battery applications. Adv. Energy Mater. 8: 1800716.

Li, Y., Li, K., Luo, Y., Liu, B., Wang, H., Gao, L., and Duan, G. (2020b). Synthesis of Co_3O_4/ZnO nano-heterojunctions by one-off processing ZIF-8@ZIF-67 and their gas-sensing performances for trimethylamine. Sens. Actuators, B 308: 127657.

Liu, C.-S., Li, J., and Pang, H. (2020). Metal-organic framework-based materials as an emerging platform for advanced electrochemical sensing. Coord. Chem. Rev. 410: 213222.

Liu, Y., Wang, R., Zhang, T., Liu, S., and Fei, T. (2019). Zeolitic imidazolate framework-8 (ZIF-8)-coated In_2O_3 nanofibers as an efficient sensing material for ppb-level NO_2 detection. J. Colloid Interface Sci. 541: 249–257.

Lu, Y., Zhan, W., He, Y., Wang, Y., Kong, X., Kuang, Q., Xie, Z., and Zheng, L. (2014). MOF-templated synthesis of porous Co_3O_4 concave nanocubes with high specific surface area and their gas sensing properties. ACS Appl. Mater. Interfaces 6: 4186–4195.

Lucero, J.M., Self, T.J., and Carreon, M.A. (2020). Synthesis of ZIF-11 crystals by microwave heating. New J. Chem. 44: 3562–3565.

Ma, Q., Chu, S., Liu, Y., Chen, Y., Song, J., Li, H., Wang, J., Che, Q., Wang, G., and Fang, Y. (2019). Construction of SnS_2/ZIF-8 derived flower-like porous SnO_2/ZnO heterostructures with enhanced triethylamine gas sensing performance. Mater. Lett. 236: 452–455.

Martinez Joaristi, A., Juan-Alcañiz, J., Serra Crespo, P., Kapteijn, F., and Gascon, J. (2012). Electrochemical synthesis of some archetypical Zn^{2+},Cu^{2+},and Al^{3+} metal organic frameworks. Cryst. Growth Des. 12: 3489–3498.

Mason, J.A., Veenstra, M., and Long, J.R. (2014). Evaluating metal–organic frameworks for natural gas storage. Chem. Sci. 5: 32–51.

Matatagui, D., Sainz-Vidal, A., Gràcia, I., Figueras, E., Cané, C., and Saniger, J.M. (2018). Chemoresistive gas sensor based on ZIF-8/ZIF-67 nanocrystals. Sens. Actuators, B 274: 601–608.

Me, D.M., Sundaram, N.G., and Kalidindi, S.B. (2018). Assembly of ZIF-67 metal-organic framework over tin oxide nanoparticles for synergistic chemiresistive CO_2 gas sensing. Chemistry 24: 9220–9223.

Meng, J., Liu, X., Niu, C., Pang, Q., Li, J., Liu, F., Liu, Z., and Mai, L. (2020). Advances in metal–organic framework coatings: versatile synthesis and broad applications. Chem. Soc. Rev. 49: 3142–3186.

Othong, J., Boonmak, J., Promarak, V., Kielar, F., and Youngme, S. (2019). Sonochemical synthesis of carbon dots/lanthanoid MOFs hybrids for white light-emitting diodes with high color rendering. ACS Appl. Mater. Interfaces 11: 44421–44429.

Pan, Y., Heryadi, D., Zhou, F., Zhao, L., Lestari, G., Su, H., and Lai, Z. (2011). Tuning the crystal morphology and size of zeolitic imidazolate framework-8 in aqueous solution by surfactants. CrystEngComm 13: 6937–6940.

Pan, Y., Li, T., Lestari, G., and Lai, Z. (2012). Effective separation of propylene/propane binary mixtures by ZIF-8 membranes. J. Membr. Sci. 390: 93–98.

Park, K., Ni, Z., Cote, A., Choi, J., Huang, R., Uribe-Romo, F., Chae, H., and KeeffeYaghi, M. (2006). Exceptional chemical and thermal stability of zeolitic imidazolate frameworks. Proc. Natl. Acad. Sci. U. S. A. 103: 10186–10191.

Pham, H., Ramos, K., Sua, A., Acuna, J., Slowinska, K., Nguyen, T., Bui, A., Weber, M.D.R., and Tian, F. (2020). Tuning crystal structures of iron-based metal–organic frameworks for drug delivery applications. ACS Omega 5: 3418–3427.

Qi, T., Yang, X., and Sun, J. (2019). Neck-connected ZnO films derived from core-shell zeolitic imidazolate framework-8 (ZIF-8)@ZnO for highly sensitive ethanol gas sensors. Sens. Actuators, B 283: 93–98.

Qian, J., Sun, F., and Qin, L. (2012). Hydrothermal synthesis of zeolitic imidazolate framework-67 (ZIF-67) nanocrystals. Mater. Lett. 82: 220–223.

Qin, C., Wang, B., Wu, N., Han, C., Wu, C., Zhang, X., Tian, Q., Shen, S., Li, P., and Wang, Y. (2020). Metal-organic frameworks derived porous Co_3O_4 dodecahedeons with abundant active Co^{3+} for ppb-level CO gas sensing. Appl. Surf. Sci. 506: 144900.

Qu, F., Jiang, H., and Yang, M. (2016). Designed formation through a metal organic framework route of ZnO/$ZnCo_2O_4$ hollow core-shell nanocages with enhanced gas sensing properties. Nanoscale 8: 16349–16356.

Qu, F., Jiang, H., and Yang, M. (2017a). MOF-derived Co_3O_4/$NiCo_2O_4$ double-shelled nanocages with excellent gas sensing properties. Mater. Lett. 190: 75–78.

Qu, F., Thomas, T., Zhang, B., Zhou, X., Zhang, S., Ruan, S., and Yang, M. (2018). Self-sacrificing templated formation of Co_3O_4/$ZnCo_2O_4$ composite hollow nanostructures for highly sensitive detecting acetone vapor. Sens. Actuators, B 273: 1202–1210.

Qu, F., Zhang, B., Zhou, X., Jiang, H., Wang, C., Feng, X., Jiang, C., and Yang, M. (2017b). Metal-organic frameworks-derived porous ZnO/$Ni_{0.9}Zn_{0.1}O$ double-shelled nanocages as gas sensing material for selective detection of xylene. Sens. Actuators, B 252: 649–656.

Reddy, A.J.M., Katari, N.K., Nagaraju, P., and Surya, S.M. (2020). ZIF-8, Zn(NA) and Zn(INA) MOFs as chemical selective sensors of ammonia, formaldehyde and ethanol gases. Mater. Chem. Phys. 241: 122357.

Ren, G., Li, Z., Yang, W., Faheem, M., Xing, J., Zou, X., Pan, Q., Zhu, G., and Du, Y. (2019). ZnO@ZIF-8 core-shell microspheres for improved ethanol gas sensing. Sens. Actuators, B 284: 421–427.

Rui, K., Wang, X., Du, M., Zhang, Y., Wang, Q., Ma, Z., Zhang, Q., Li, D., Huang, X., Sun, G., et al. (2018). Dual-function metal-organic framework-based wearable fibers for gas probing and energy storage. ACS Appl. Mater. Interfaces 10: 2837–2842.

Salunkhe, R.R., Kaneti, Y.V., and Yamauchi, Y. (2017). Metal–organic framework-derived nanoporous metal oxides toward supercapacitor applications: progress and prospects. ACS Nano 11: 5293–5308.

Shen, K., Chen, X., Chen, J., and Li, Y. (2016). Development of MOF-derived carbon-based nanomaterials for efficient catalysis. ACS Catal. 6: 5887–5903.

Soleimani, M., Abbasi, A., and Najafi, M. (2020). Preparation of micro and nanorod metal organic framework through coordination modulation method as precursor for micro and nanorod NiO. J. Inorg. Organomet. Polym. 30: 596–602.

Soltanolkottabi, F., Talaie, M.R., Aghamiri, S., and Tangestaninejad, S. (2020). The effect of reaction mixture movement on the performance of chromium-benzenedicarboxylate, MIL-101(Cr), applicable for CO_2 adsorption through a new circulating solvothermal synthesis process. J. Iran. Chem. Soc. 17: 17–24.

Song, F., Cao, Y., Zhao, Y., Jiang, R., Xu, Q., Yan, J., and Zhong, Q. (2020). Ion-exchanged ZIF-67 synthesized by one-step method for enhancement of CO_2 adsorption. J. Nanomater. 20: 1–11.

Stock, N. and Biswas, S. (2012). Synthesis of metal-organic frameworks (MOFs): routes to various MOF topologies, morphologies, and composites. Chem. Rev. 112: 933–969.

Sun, C.Y., Qin, C., Wang, X.L., Yang, G.S., Shao, K.Z., Lan, Y.Q., Su, Z.M., Huang, P., Wang, C.G., and Wang, E.B. (2012). Zeolitic Imidazolate framework-8 as efficient pH-sensitive drug delivery vehicle. Dalton Trans. 41: 6906–6909.

Taheri, M., Ashok, D., Sen, T., Enge, T.G., Verma, N.K., Tricoli, A., Lowe, A., Nisbet, R.D., and Tsuzuki, T. (2021). Stability of ZIF-8 nanopowders in bacterial culture media and its implication for antibacterial properties. Chem. Eng. J. 413: 127511.

Tai, H., Wang, S., Duan, Z., and Jiang, Y. (2020). Evolution of breath analysis based on humidity and gas sensors: potential and challenges. Sens. Actuators, B 318: 128104.

Tan, J., Hussain, S., Ge, C., Wang, M., Shah, S., Liu, G., and Qiao, G. (2020). ZIF-67 MOF-derived unique double-shelled Co_3O_4/$NiCo_2O_4$ nanocages for superior gas-sensing performances. Sens. Actuators, B 303: 127251.

The Ky, V., Van Nhieu, L., Yoo, K.S., Song, M., Kim, D., and Kim, J. (2019). Facile synthesis of UiO-66(Zr) using a microwave-assisted continuous tubular reactor and its application for toluene adsorption. Cryst. Growth Des. 19: 4949–4956.

Tian, H., Fan, H., Li, M., and Ma, L. (2015). Zeolitic imidazolate framework coated ZnO nanorods as molecular sieving to improve selectivity of formaldehyde gas sensor. ACS Sens. 1: 243–250.

Tian, L., Sun, Y., Huang, H., Guo, X., Qiao, Z., Meng, J., and Zhong, C. (2020). Porous ZIF-8 thin layer coating on ZnO hollow nanofibers for enhanced acetone sensing. ChemistrySelect 5: 2401–2407.

Tsai, C.W., Niemantsverdriet, J.W., and Langner, E.H.G. (2018). Enhanced CO_2 adsorption in nano-ZIF-8 modified by solvent assisted ligand exchange. Microporous Mesoporous Mater. 262: 98–105.

Wales, D.J., Grand, J., Ting, V.P., Burke, R.D., Edler, K.J., Bowen, C.R., Mintova, S., and Burrows, A.D. (2015). Gas sensing using porous materials for automotive applications. Chem. Soc. Rev. 44: 4290–4321.

Wang, C., Kaneti, Y.V., Bando, Y., Lin, J., Liu, C., Li, J., and Yamauchi, Y. (2018a). Metal–organic framework-derived one-dimensional porous or hollow carbon-based nanofibers for energy storage and conversion. Mater. Horiz. 5: 394–407.

Wang, M., Shen, Z., Zhao, X., Duanmu, F., Yu, H., and Ji, H. (2019). Rational shape control of porous Co_3O_4 assemblies derived from MOF and their structural effects on n-butanol sensing. J. Hazard Mater. 371: 352–361.

Wang, P., Zou, X., Tan, H., Wu, S., Jiang, L., and Zhu, G. (2018b). Ultrathin ZIF-8 film containing polyoxometalate as an enhancer for selective formaldehyde sensing. J. Mater. Chem. C 6: 5412–5419.

Wang, S., Mcguirk, C.M., D'aquino, A., Mason, J.A., and Mirkin, C.A. (2018c). Metal-organic framework nanoparticles. Adv. Mater. 30: 1800202.

Weber, M., Kim, J.H., Lee, J.H., Kim, J.Y., Iatsunskyi, I., Coy, E., Drobek, M., Julbe, A., Bechelany, M., and Kim, S.S. (2018). High-performance nanowire hydrogen sensors by exploiting the synergistic effect of Pd nanoparticles and metal–organic framework membranes. ACS Appl. Mater. Interfaces 10: 34765–34773.

Wojnowski, W., Majchrzak, T., Dymerski, T., Gebicki, J., and Namiesnik, J. (2017). Portable electronic nose based on electrochemical sensors for food quality assessment. Sensors 17: 2715.

Wu, S., Xin, Z., Zhao, S., and Sun, S. (2019a). High-throughput droplet microfluidic synthesis of hierarchical metal-organic framework nanosheet microcapsules. Nano Res. 12: 2736–2742.

Wu, W., Zhang, Z., Lei, Z., Wang, X., Tan, Y., Cheng, N., and Sun, X. (2020). Encapsulating Pt nanoparticles inside a derived two-dimensional metal-organic frameworks for the enhancement of catalytic activity. ACS Appl. Mater. Interfaces 12: 10359–10368.

Wu, X., Xiong, S., Gong, Y., Gong, Y., Wu, W., Mao, Z., Liu, Q., Hu, S., and Long, X. (2019b). MOF-SMO hybrids as a H_2S sensor with superior sensitivity and selectivity. Sens. Actuators, B 292: 32–39.

Wu, X., Xiong, S., Mao, Z., Hu, S., and Long, X. (2017). A designed ZnO@ZIF-8 core-shell nanorod film as a gas sensor with excellent selectivity for H_2 over CO. Chemistry 23: 7969–7975.

Xia, J., Diao, K., Zheng, Z., and Cui, X. (2017). Porous Au/ZnO nanoparticles synthesised through a metal organic framework (MOF) route for enhanced acetone gas-sensing. RSC Adv. 7: 38444–38451.

Xiao, J., Diao, K., Zheng, Z., and Cui, X. (2018). MOF-derived porous ZnO/Co_3O_4 nanocomposites for high performance acetone gas sensing. J. Mater. Sci. Mater. Electron. 29: 8535–8546.

Xiong, Y., Xu, W., Zhu, Z., Xue, Q., Lu, W., Ding, D., and Zhu, L. (2017). ZIF-derived porous $ZnO\text{-}Co_3O_4$ hollow polyhedrons heterostructure with highly enhanced ethanol detection performance. Sens. Actuators, B 253: 523–532.

Xu, K., Zhao, W., Yu, X., Duan, S., and Zeng, W. (2020a). MOF-derived Co_3O_4/Fe_2O_3 p–n hollow cubes for improved acetone sensing characteristics. Physica E 118: 113869.

Xu, X., Sun, Y., Zhang, Q., Wang, S., Zhang, L., Wu, Z., and Lu, G. (2016). Synthesis of ZIF-8 hollow spheres via MOF-to-MOF conversion. ChemistrySelect 1: 1763–1767.

Xu, X., Wang, H., Liu, J., and Yan, H. (2017). The applications of zeolitic imidazolate framework-8 in electrical energy storage devices: a review. J. Mater. Sci. Mater. Electron. 28: 7532–7543.

Xu, X., Zhao, C., Liu, X., Liu, Y., Dong, P., and Itani, C. (2020b). Metal-organic framework-derived $ZnMoO_4$ nanosheet arrays for advanced asymmetric supercapacitors. J. Mater. Sci. Mater. Electron. 31: 3631–3641.

Yan, H., Xie, Y., Jiao, Y., Wu, A., Tian, C., Zhang, X., Wang, L., and Fu, H. (2018). Holey reduced graphene oxide coupled with an Mo_2N–Mo_2C heterojunction for efficient hydrogen evolution. Adv. Mater. 30: 1704156.

Yang, J. and Yang, Y.W. (2020). Metal-organic frameworks for biomedical applications. Small 16: 1906846.

Yao, M.S., Cao, L.A., Tang, Y.X., Wang, G.E., Liu, R.H., Kumar, P.N., Wu, G.D., Deng, W.H., Hong, W.J., and Xu, G. (2019). Gas transport regulation in a MO/MOF interface for enhanced selective gas detection. J. Mater. Chem. A. 7: 18397–18403.

Ying, Y., Xiao, Y., Ma, J., Guo, X., Huang, H., Yang, Q., Liu, D., and Zhong, C. (2015). Recovery of acetone from aqueous solution by ZIF-7/PDMS mixed matrix membranes. RSC Adv. 5: 28394–28400.

Yu, D., Ge, L., Wu, B., Wu, L., Wang, H., and Xu, T. (2015). Precisely tailoring ZIF-67 nanostructures from cobalt carbonate hydroxide nanowire arrays: toward high-performance battery-type electrodes. J. Mater. Chem. A. 3: 16688–16694.

Yu, L., Yang, J.F., and Lou, X.W. (2016). Formation of CoS_2 nanobubble hollow prisms for highly reversible lithium storage. Angew. Chem. Int. Ed. 55: 13422–13426.

Yuan, S., Feng, L., Wang, K., Pang, J., Bosch, M., Lollar, C., Sun, Y., Qin, J., Yang, X., Zhang, P., et al. (2018). Stable metal-organic frameworks: design, synthesis, and applications. Adv. Mater. 30: 1704303.

Zakzeski, J., Dębczak, A., Bruijnincx, P.C.A., and Weckhuysen, B.M. (2011). Catalytic oxidation of aromatic oxygenates by the heterogeneous catalyst Co-ZIF-9. Appl. Catal, A 394: 79–85.

Zhang, D., Wu, Z., and Zong, X. (2019a). Metal-organic frameworks-derived zinc oxide nanopolyhedra/S, N:graphene quantum dots/polyaniline ternary nanohybrid for high-performance acetone sensing. Sens. Actuators, B 288: 232–242.

Zhang, D., Yang, Z., Wu, Z., and Dong, G. (2019b). Metal-organic frameworks-derived hollow zinc oxide, cobalt oxide nanoheterostructure for highly sensitive acetone sensing. Sens. Sens. Actuators, B 283: 42–51.

Zhang, H., Wang, C., Zhang, W., Zhang, M., Qi, J., Qian, J., Sun, X., Yuliarto, B., Na, J., Park, T., et al. (2021). Nitrogen, phosphorus co-doped eave-like hierarchical porous carbon for efficient capacitive deionization. J. Mater. Chem. A. 9: 12807–12817.

Zhang, J., Lu, H., Zhang, L., Leng, D., Zhang, Y., Wang, W., Gao, Y., Lu, H., Gao, J., Zhu, G., et al. (2019c). Metal–organic framework-derived ZnO hollow nanocages functionalized with nanoscale Ag catalysts for enhanced ethanol sensing properties. Sens. Actuators, B 291: 458–469.

Zhang, J., Tan, Y., and Song, W.J. (2020a). Zeolitic imidazolate frameworks for use in electrochemical and optical chemical sensing and biosensing: a review. Microchim. Acta 187: 234.

Zhang, N., Ruan, S., Qu, F., Yin, Y., Li, X., Wen, S., Adimi, S., and Yin, J. (2019d). Metal–organic framework-derived $Co_3O_4/CoFe_2O_4$ double-shelled nanocubes for selective detection of sub-ppm-level formaldehyde. Sens. Actuators, B 298: 126887.

Zhang, R., Song, W., Wang, M., and Ji, H. (2019e). Controlling the size of a Zn-MOF through ligand exchange and pore-tailored ZnO assemblies for size-selective gas sensing. CrystEngComm 21: 6414–6422.

Zhang, R., Zhou, T., Wang, L., and Zhang, T. (2018a). Metal-organic frameworks-derived hierarchical Co_3O_4 structures as efficient sensing materials for acetone detection. ACS Appl. Mater. Interfaces 10: 9765–9773.

Zhang, T., Tang, X., Zhang, J., Zhou, T., Wang, H., Wu, C., Xia, X., Xie, C., and Zeng, D. (2018b). Metal-organic framework-assisted construction of TiO_2/Co_3O_4 highly ordered necklace-like heterostructures for enhanced ethanol vapor sensing performance. Langmuir 34: 14577–14585.

Zhang, X., Chen, A., Zhong, M., Zhang, Z., Zhang, X., Zhou, Z., and Bu, X.H. (2019f). Metal–organic frameworks (MOFs) and MOF-derived materials for energy storage and conversion. Electrochem. Energy Rev. 2: 29–104.

Zhang, X., Lan, W., Xu, J., Luo, Y., Pan, J., Liao, C., Yang, L., Tan, W., and Huang, X. (2019g). ZIF-8 derived hierarchical hollow ZnO nanocages with quantum dots for sensitive ethanol gas detection. Sens. Actuators, B 289: 144–152.

Zhang, X., Wang, J., Ji, X., Sui, Y., Wei, F., Qi, J., Meng, Q., Ren, Y., and He, Y. (2020b). Nickel/cobalt bimetallic metal-organic frameworks ultrathin nanosheets with enhanced performance for supercapacitors. J. Alloys Compd. 825: 154069.

Zhang, X., Xu, Y., Liu, H., Zhao, W., Ming, A., and Wei, F. (2020c). Preparation of porous Co_3O_4 and its response to ethanol with low energy consumption. RSC Adv. 10: 2191–2197.

Zhou, H., Zhang, J., Zhang, J., Yan, X., Shen, X., and Yuan, A. (2015). High-capacity room-temperature hydrogen storage of zeolitic imidazolate framework/graphene oxide promoted by platinum metal catalyst. Int. J. Hydrogen Energy 40: 12275–12285.

Zhou, H., Zheng, M., Tang, H., Xu, B., Tang, Y., and Pang, H. (2020a). Amorphous intermediate derivative from ZIF-67 and its outstanding electrocatalytic activity. Small 16: 1904252.

Zhou, K., Mousavi, B., Luo, Z., Phatanasri, S., Chaemchuen, S., and Verpoort, F. (2017). Characterization and properties of Zn/Co zeolitic imidazolate frameworks versus ZIF-8 and ZIF-67. J. Mater. Chem. A. 5: 952–957.

Zhou, X., Lin, X., Yang, S., Zhu, S., Chen, X., Dong, B., Bai, X., Wen, X., Lu, G., and Song, H. (2020b). Highly dispersed metal–organic-framework-derived Pt nanoparticles on three-dimensional macroporous ZnO for trace-level H_2S sensing. Sens. Actuators, B 309: 127802.